Improvement and Uncertainties of Global Simulation of Sulfate Concentration and Radiative Forcing in CESM2

Wendong Ge[1], Junfeng Liu[1], Songlin Xiang[2], Yuhan Zhou[1], Jingcheng Zhou[1], Xiurong Hu[2], Jianmin Ma[2], Xuejun WANG[2], Yi Wan[1], Jianying Hu[1], Zhaobin Zhang[1], Xilong Wang[2], and Shu Tao[2]

[1]College of Urban and Environmental Sciences, Peking University
[2]Peking University

November 24, 2022

Abstract

Sulfate is a major atmospheric pollutant and radiative forcing (RF) factor that influences air quality, cloud microphysics and climate. Therefore, a better evaluation of sulfate concentrations and RF patterns is essential for policy-making and the management of air pollution and climate change. This study comprehensively estimates the global distribution of sulfate concentrations and RFs and analyzes the sources of uncertainty in the Community Earth System Model version 2 (CESM2) and the Parallel Offline Radiative Transfer (PORT) model. Compared with the observations, the incorporation of detailed in-cloud aqueous-phase chemistry and the enhanced wet deposition flux of sulfate significantly improved the simulations of sulfur species both near the ground and at high altitudes, which is beneficial for a more accurate estimation of the global sulfate RF. The improved simulated RF of sulfate from 1850 to 2015 is -0.382 $W.m^{-2}$. This study finds that wet deposition is the key process governing both the horizontal and vertical distributions of sulfate concentrations. The overestimation of surface sulfate and the underestimation of high-altitude sulfate made by the model are essential uncertainty factors of the sulfate RF estimation. This study emphasizes the importance of improving the simulation of global sulfate distribution as well as its RF, which may strongly pressure the near-future warming potential when witnessing a rapid transition to a carbon neutral world that is phasing out fossil fuel. A more accurate assessment of sulfate levels and radiation effects will play a remarkable guiding role in the formulation of global emission reduction-related policies in the future.

Improvement and Uncertainties of Global Simulation of Sulfate Concentration and Radiative Forcing in CESM2

Wendong Ge[1], Junfeng Liu[1], Songlin Xiang[1], Yuhan Zhou[1], Jingcheng Zhou[1], Xiurong Hu[2], Jianmin Ma[1], Xuejun Wang[1], Yi Wan[1], Jianying Hu[1], Zhaobin Zhang[1], Xilong Wang[1], Shu Tao[1]

[1]Laboratory for Earth Surface Processes, College of Urban and Environmental Sciences, Peking University, Beijing, 100871, China

[2] College of Economics and Management, Nanjing University of Aeronautics and Astronautics, Nanjing, 211106, China

Corresponding author: Junfeng Liu (jfliu@pku.edu.cn)

Key Points:

- The global simulations of sulfate distribution and radiative forcing are significantly improved with the usage of CESM2.
- Wet deposition is the key process governing both the horizontal and vertical distributions of global sulfate concentrations.
- The uncertainty of sulfate forcing is very important to the formulation of global carbon neutral policies.

Abstract

Sulfate is a major atmospheric pollutant and radiative forcing (RF) factor that influences air quality, cloud microphysics and climate. Therefore, a better evaluation of sulfate concentrations and RF patterns is essential for policy-making and the management of air pollution and climate change. This study comprehensively estimates the global distribution of sulfate concentrations and RFs and analyzes the sources of uncertainty in the Community Earth System Model version 2 (CESM2) and the Parallel Offline Radiative Transfer (PORT) model. Compared with the observations, the incorporation of detailed in-cloud aqueous-phase chemistry and the enhanced wet deposition flux of sulfate significantly improved the simulations of sulfur species both near the ground and at high altitudes, which is beneficial for a more accurate estimation of the global sulfate RF. The improved simulated RF of sulfate from 1850 to 2015 is -0.382 $W \cdot m^{-2}$. This study finds that wet deposition is the key process governing both the horizontal and vertical distributions of sulfate concentrations. The overestimation of surface sulfate and the underestimation of high-altitude sulfate made by the model are essential uncertainty factors of the sulfate RF estimation. This study emphasizes the importance of improving the simulation of global sulfate distribution as well as its RF, which may strongly pressure the near-future warming potential when witnessing a rapid transition to a carbon neutral world that is phasing out fossil fuel. A more accurate assessment of sulfate levels and radiation effects will play a remarkable guiding role in the formulation of global emission reduction-related policies in the future.

Plain Language Summary

Sulfate aerosols play an essential role in the entire atmosphere and climate system. Therefore, it is necessary to better simulate the distribution and radiative forcing of sulfate. By using a global climate model, we improved the simulation of sulfate distribution both near the ground and at high altitudes and achieved a more accurate estimation of the global radiative forcing of sulfate. We found that wet deposition is the key process influencing the distribution of sulfate concentrations. The overestimation of surface sulfate and the underestimation of high-altitude sulfate are important uncertainty factors of sulfate radiative forcing. Our results suggest that more field studies (e.g., aircraft campaigns, surface measurements over remote regions, etc.) of sulfate are urgently needed. This study indicates that large uncertainties may exist in current global climate models, which may impact the formulation of future policy-making in carbon neutrality.

1 Introduction

Sulfate is one of the major species of aerosol. Both natural sources (such as oxidation of dimethyl sulfur (DMS)) over the ocean and anthropogenic emissions of sulfur dioxide (SO_2) are important sources of sulfate (Hussain & Lun, 2019; Sanchez et al., 2018; Yan & Xu, 2021). Human industrial activities have increased significantly since the industrial era, and the gas-phase, liquid-phase and surface heterogeneous oxidations of SO_2 have gradually accounted for the main sources of sulfate (B. Liu et al., 2017; Xue et al., 2016). As an important component of atmospheric particulate matter (PM), sulfate at high concentrations will aggravate the formation of haze, thus causing serious air pollution and influencing human health (Sha et al., 2019; B. Zheng et al., 2015; Zhou et al., 2020). Moreover, sulfate is also one of the main species of acid deposition, reducing the pH values of rain droplets and aggravating acid rain (M. Liu et al., 2020; Lu, Fung, & Wu, 2015; K. Zheng et al., 2019). At the same time, sulfate is also the main

component of cloud condensation nuclei (CCN), which affects microphysical processes, including the formation of clouds and precipitation, thus affecting solar radiation and climate (Cziczo et al., 2013). Furthermore, sulfate itself is also one of the key short-lived species that has negative radiative forcing (RF), which could influence the climate directly (Richardson et al., 2019). Therefore, sulfate plays an essential role in the entire atmosphere and climate system.

In view of the fundamental roles of sulfate in many related fields, previous studies on sulfate have made extensive, in-depth progress in recent decades. First, most regional atmospheric monitoring studies have fully analyzed the appearance, source, temporal fluctuation and spatial distribution of sulfate, as well as its proportion in PM. At the same time, modeling studies have made great advances in revealing various mechanisms of SO_2 oxidation and sulfate formation under different conditions and have greatly improved the performance of sulfate simulation (Gao et al., 2016; G. Li et al., 2017; Luo, Yu, & Moch, 2020; Shao et al., 2019). For instance, multiple studies emphasized the importance of aqueous-phase oxidation catalyzed by transition metals in haze episodes (X. Huang et al., 2014; J. Li et al., 2020; Wang et al., 2021), while other studies interpreted heterogeneous oxidation by NO_2 or HONO on the aerosol surface as the dominant pathway, especially under conditions of high pH values and high NH_3 concentrations (Cheng et al., 2016; L. Huang et al., 2019; Yue et al., 2019; H. Zheng et al., 2020). Some studies also analyzed the potential enhancement of sulfate formation by black carbon (BC) (F. Zhang et al., 2020). In addition, wet deposition (WD) is the dominant removal process for sulfate, accounting for more than 90% of its sink (Dentener et al., 2006; Driscoll, Driscoll, Fakhraei, & Civerolo, 2016; B. Li et al., 2018; Qiao et al., 2015). Multiple studies have discussed the simulation and observation of sulfate wet deposition in different regions and periods, illustrating its great fluctuation and uncertainty in different models (Conradie et al., 2016; Horowitz, 2006; Keene et al., 2015; Luo et al., 2020).

Furthermore, more studies have focused on RF and the climate response of sulfate. Some of them discussed the sulfate RF both from anthropogenic sources and volcanic eruptions in the upper troposphere and stratosphere (Aubry et al., 2021; C.-C. Chen & Gettelman, 2016; Flanner, Gardner, Eckhardt, Stohl, & Perket, 2014; B. Li et al., 2018). Li et al. (2016) compared the cooling effect of sulfate and warming effect of CO_2 and BC in China and concluded that the negative RF of sulfate from intensive power and industry activities has offset most of the warming factors. In contrast, studies have emphasized the weakened cooling effect or even warming effect due to the rapid reduction in SO_2 emissions in China (Kasoar et al., 2016; M. Liu & Matsui, 2021; X.-x. Ma, Liu, Wang, & Zhang, 2016). Moreover, sensitivity tests are often used for sulfate to estimate its influence on global temperature and precipitation (e.g., increasing the sulfate concentration to 5 or 10 times or removing anthropogenic SO_2 emissions) (Asutosh, Fadnavis, Nuncio, Mueller, & Tripathy, 2021; Kasoar et al., 2016; L. Liu et al., 2018; Shawki, Voulgarakis, Chakraborty, Kasoar, & Srinivasan, 2018).

However, all the studies mentioned above are still insufficient, especially in the performance of sulfate simulation. First, although the surface monitoring networks in most regions of the world have been gradually established and improved in recent years, the aircraft measurement campaigns of sulfate are still relatively insufficient. For model studies, some of them could only roughly reproduce the seasonal pattern of sulfate but had obvious biases in simulating the magnitude of both near-surface concentrations and vertical distribution (Yang, Wang, Smith, Easter, & Rasch, 2018). Although the chemical mechanisms have improved remarkably, there are still significant overestimations of sulfate in different regions and seasons

in many regional and global models (Breider et al., 2017; Buchard et al., 2014; Georgiou et al., 2018; Lamarque et al., 2012; Lee et al., 2020; X. Li & Liu, 2013; X. Liu et al., 2012; Xiaohong Liu et al., 2007; Sobhani, Kulkarni, & Carmichael, 2018; Wei et al., 2019; Wu et al., 2020; Yang et al., 2018; B. Zhang et al., 2019). On the one hand, it may be related to the rapid reduction in SO_2 and sulfate emissions in many regions (especially in Europe, the United States (US) and China) during recent years, which has resulted in the sharp decline in the observed concentration of sulfate (de Meij et al., 2006; Fedkin, Li, Dickerson, Canty, & Krotkov, 2019; Syuichi Itahashi et al., 2018; H. Li et al., 2019; McClure & Jaffe, 2018; Sickles & Shadwick, 2015; Xie, Liu, Wang, & Wang, 2016). On the other hand, considering that the wet deposition of sulfate is derived from cloud formation and has great uncertainty (Breider et al., 2017; Z. Chen et al., 2019; Dentener et al., 2006; Echeverria, Abreu, Gonzalez, Ortega, & Echeverria, 2016; Horowitz, 2006; Luo et al., 2020), it also tends to be underestimated in some studies (S. Itahashi, 2018; Sedefian, Ku, Civerolo, Hao, & Zalewsky, 2016; Vivanco et al., 2017). An analysis of modeling studies suggests that the greatest uncertainty in global sulfur cycling is derived from the wet deposition of aerosol sulfate and the heterogeneous oxidation of SO_2 in clouds and aerosols (Faloona, 2009). As a result, the further evaluation of RF and the climate response of sulfate is likely to contain great uncertainty (Goto, Nakajima, Takemura, & Sudo, 2011; Ming, Ramaswamy, Ginoux, Horowitz, & Russell, 2005; Paulot, Paynter, Ginoux, Naik, & Horowitz, 2018; Stevens, 2015; Thornhill et al., 2021; Yang et al., 2017). Therefore, it is necessary to conduct further research on the simulation of sulfate concentration and RF and analyze the factors that lead to their uncertainties in detail.

This study aims to comprehensively evaluate and improve the performance of sulfate simulation in the Community Earth System Model 2 (CESM2), estimate the global RF of sulfate with the Parallel Offline Radiative Transfer (PORT) model, and, on this basis, discuss the factors influencing the simulation of sulfate concentration and RF. The descriptions of the CESM2 and PORT configuration as well as the observational data are introduced in section 2. The evaluation of sulfate simulations both near the ground and at high altitude will be shown in section 3. Next, the global RF of sulfate is estimated in section 4. Then, section 5 discusses the uncertainties associated with our simulations. Finally, key conclusions are presented in section 6.

2 Methodology

2.1 Model description

The simulations in this study are conducted with the Community Earth System Model 2 (CESM2 v2.1.3) (Danabasoglu et al., 2020; Louisa K. Emmons et al., 2020) and the Parallel Offline Radiative Transfer (PORT) model (Conley, Lamarque, Vitt, Collins, & Kiehl, 2013), both developed by the National Center for Atmospheric Research (NCAR, https://www.cesm.ucar.edu/models/cesm2/, last access: 13 June 2022). The CESM2 is a fully coupled global climate model configured with Community Atmosphere Model version 4.0 (CAM4) and coupled with the chemistry of Model for Ozone and Related chemical Tracers version 4 (MOZART-4) in this study (L. K. Emmons et al., 2010; Lamarque et al., 2012). Furthermore, we also incorporated a detailed in-cloud aqueous-phase chemistry module into MOZART-4 chemistry in the improved cases illustrated below, referring to the study of Ge et al. (2021).

The PORT model is a stand-alone radiative transfer model isolated with the CAM in the CESM so that radiative fluxes can be computed without feedback on the surface. PORT can be used for any radiation calculation. It implements stratospheric temperature adjustment under the assumption of fixed dynamical heating, which is necessary for the computation of RF and instantaneous radiative forcing (IRF) (Conley et al., 2013). Updated physics (CAM5) and a radiation scheme (RRTMG) are used in this study.

Both models are configured with a horizontal resolution of 0.95° latitude and 1.25° longitude and 30 levels from approximately 993 (near-surface layer) to 3.6 hPa in the vertical direction. The offline meteorological data for model nudging are obtained from the Modern-Era Retrospective analysis for Research and Applications version 2 (MERRA2, https://rda.ucar.edu/datasets/ds313.3/, last access: 13 June 2022) (Gelaro et al., 2017; Molod, Takacs, Suarez, & Bacmeister, 2015), all of whose temporal resolution is 3 h. All the emission inventories needed for both models are obtained from the CESM database developed for CMIP6 projects (https://svn-ccsm-inputdata.cgd.ucar.edu/trunk/inputdata/atm/cam/chem/emis/emissions_ssp245/, last access: 13 June 2022) (L. Feng et al., 2020; Hoesly et al., 2018; McDuffie et al., 2020; Steven, Yuyu, & Page, 2015). These inventories include both historical emissions from as early as 1750 to 2015 (annual) and predicted emissions from 2020 to 2100 (decade) under different climate scenarios and are thus in accordance with the demands of the simulation periods in this study.

2.2 Model configuration

The basic information of all simulations conducted in this study is summarized in Table S1. First, we conducted the simulation without any modification to the model (i.e., the Original case). Then, the default parameterized SO_2 aqueous-phase reactions in the Original model were replaced with detailed in-cloud aqueous-phase chemical mechanisms (Ge et al., 2021). Furthermore, considering the high uncertainty of sulfate wet deposition parameterization in models, a series of sensitivity simulations of sulfate wet deposition flux with different adjustments (increased by factors of 5, 10, 15 and 20 (i.e., the Improved case)) were performed to further optimize the simulation performance (Dentener et al., 2006; Horowitz, 2006).

On the basis of the Original and Improved simulations of CESM, the PORT model was performed to determine the RF of sulfate. PORT is driven by model-generated datasets. In addition to the datasets mentioned above, PORT also requires the sulfate concentrations simulated by CESM cases as input files and then simulates and calculates the RF of sulfate through the differences in its concentrations between different CESM cases. Therefore, we further replaced the SO_2 emissions with their corresponding inventories in the preindustrial period (1849-1850) and then simulated the global distributions of sulfate concentrations both in the preindustrial period and without anthropogenic sources and their corresponding RFs with PORT cases (Carslaw et al., 2017; Shawki et al., 2018; Smith et al., 2020; Thornhill et al., 2021). Finally, in consideration of the factors that increase the uncertainty of sulfate RF simulation, a series of sensitivity tests with the PORT model were conducted, which will be illustrated in section 5 in detail.

Ultimately, all the simulations of this study run for a two-year period from 1 January 2014 to 31 December 2015, which is representative of the present day, or from 1 January 1849 to 31 December 1850, which is representative of the preindustrial era. The first year (2014 or 1849) is used for model spin-up. The timestep used in both CESM and PORT is the default of 30

minutes. The output of the CESM simulation is the daily mean and is then converted to monthly or seasonal means for analysis. The time interval of the input files of PORT is a default of 73 timesteps (i.e., 36.5 hours), and the output RF used in this study is in the form of a monthly mean and is converted to an annual mean for analysis.

2.3 Surface monitoring networks and aircraft measurement campaigns

To better evaluate the performance of the model in simulating sulfate concentrations, the observed data used in this study are collected from three surface monitoring networks and three aircraft measurement campaigns. The locations of surface monitoring stations of different networks and the flight regions and tracks of different aircraft campaigns are shown in Figure 1. For surface observations, the data in Europe (EU) are obtained from the European Monitoring and Evaluation Programme (EMEP, https://www.emep.int/, last access: 14 June 2022). The observations in the US are obtained from the Interagency Monitoring of Protected Visual Environments (IMPROVE, http://vista.cira.colostate.edu/Improve/, last access: 14 June 2022). The observations in east and south Asia (EA and SA) are obtained from the Acid Deposition Monitoring Network in East Asia (EANET, https://monitoring.eanet.asia/document/public/index, last access: 14 June 2022). With regard to the aircraft observations, the Atmospheric Tomography Mission data (ATom, https://daac.ornl.gov/cgi-bin/dsviewer.pl?ds_id=1925, last access: 14 June 2022) are mostly measured over the ocean (Wofsy et al., 2021). The Wintertime Investigation of Transport, Emission, and Reactivity observations (WINTER, https://data.eol.ucar.edu/dataset/483.025, last access: 14 June 2022) are mainly carried out over the sea and land of the eastern US (Green et al., 2019). The International Cooperative Air Quality Field Study in Korea (KORUS-AQ, https://espo.nasa.gov/korus-aq/content/KORUS-AQ, last access: 14 June 2022) is concentrated around South Korea (Lee et al., 2020).

All the surface observational data were directly collected from 1 January 2015 to 31 December 2015 in the form of daily averages and were further converted to monthly averages for analysis. However, the aircraft measurements are relatively limited, and the observation year and date may not match those of the simulation. Because the sulfate concentration in the same period of adjacent years will not change significantly in terms of the order of magnitude, all the simulated concentrations of sulfate were uniformly selected on the corresponding dates in 2015 for comparison. The flight dates of all aircraft measurements referred to in this study are listed in Figures 3 and S2. For the convenience of comparison, the aircraft observed concentrations of each flight were averaged by different altitude segments within the whole rectangular region as defined in Figure 1. Then, the simulated concentrations were daily averages within the whole rectangular flight region in each layer that covered the height range of the corresponding aircraft measurements (J. Liu, Fan, Horowitz, & Levy, 2011). To make the comparison more representative, these aircraft measurements cover different regions (as described above), altitudes (approximately 2 km to 13 km) and months (March to August).

3 Improvements of global sulfate simulations

3.1 Differences in sulfate concentrations between the Original and Improved simulations

First, the seasonally averaged global distribution of the sulfate surface concentration simulated in the Original case is shown in Figure 2, which exhibits significant spatial variability. Most sulfate is concentrated in continental regions of the Northern Hemisphere, including

Europe (EU), North America (NAM), EA and SA, mainly from anthropogenic SO_2 emissions, such as energy and industrial activities), the Middle East (ME) and North Africa (NAF, mainly from natural sources). The sulfate concentrations in most of these regions exceed 5 $\mu g \cdot m^{-3}$ and even 20 $\mu g \cdot m^{-3}$ in some regions, especially in China and India, indicating pollution from intensive industrial activities. On the other hand, the sulfate concentrations are relatively low over oceans and generally less than 5 $\mu g \cdot m^{-3}$ in most regions, mainly from the oxidation of DMS.

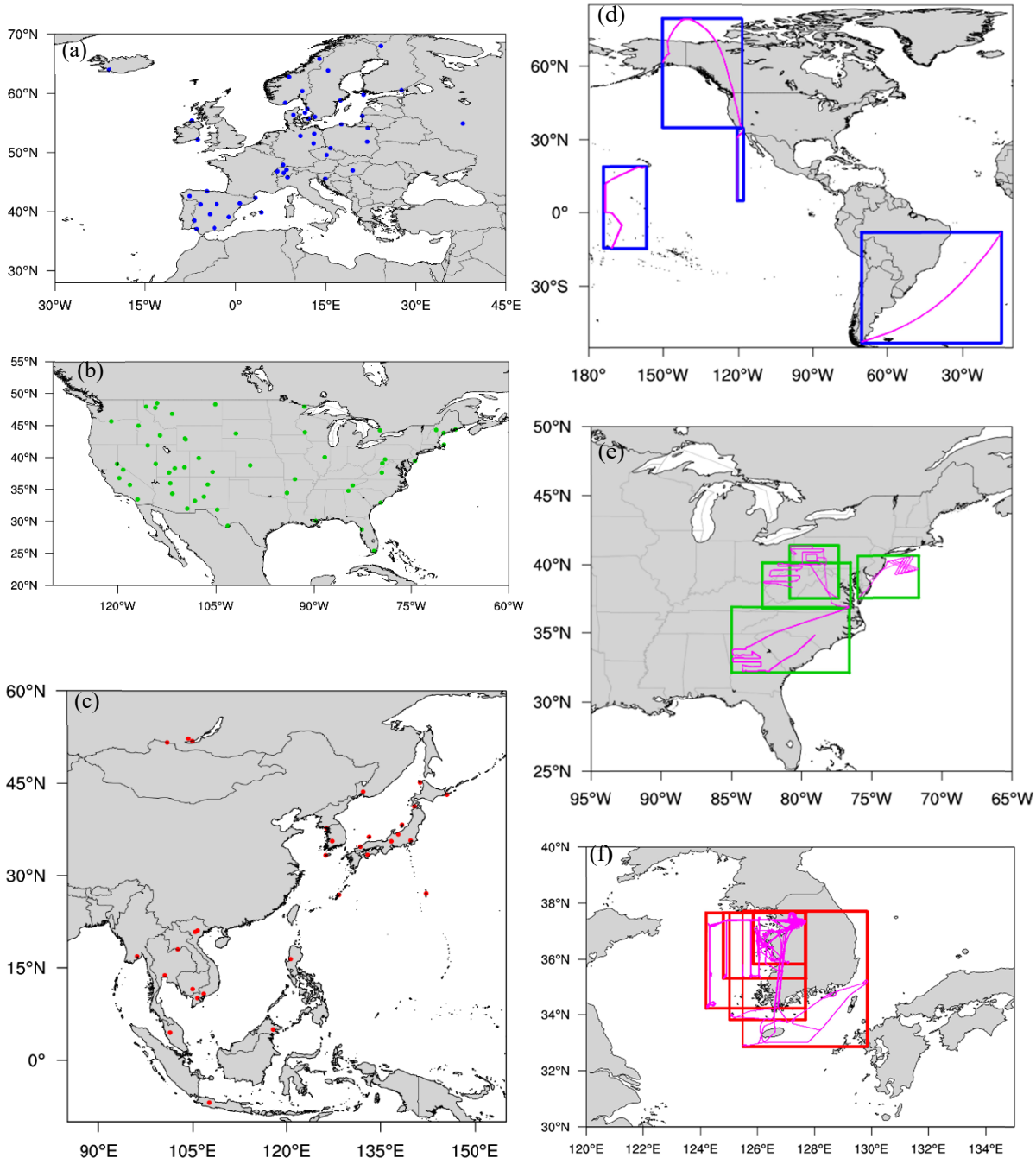

Figure 1. Locations of monitoring sites from three surface measurement networks in (a) EU (EMEP), (b) US (EPA) and (c) EA and flight ranges of three aircraft measurement campaigns, including (d) ATom, (e) WINTER and (f) KORUS-AQ, at different times. The pink lines are the tracks of each flight.

In terms of seasons, however, there is no significant and consistent distributional characteristic worldwide. In general, the concentrations in both hemispheres are slightly higher in spring and summer than in autumn and winter but do not fluctuate intensively in different seasons, which is obviously different from that of SO_2 (Ge et al., 2021). Such differences are related to the combination of precursor emissions and atmospheric oxidation capacity. In summer, the sulfur emissions are relatively weak due to the decreased demand for heating. Sufficient sunlight and high temperature in summer enhance the oxidation capacity at the same time, which promotes the formation of ·OH radicals and sulfate. These simulations are the opposite in winter.

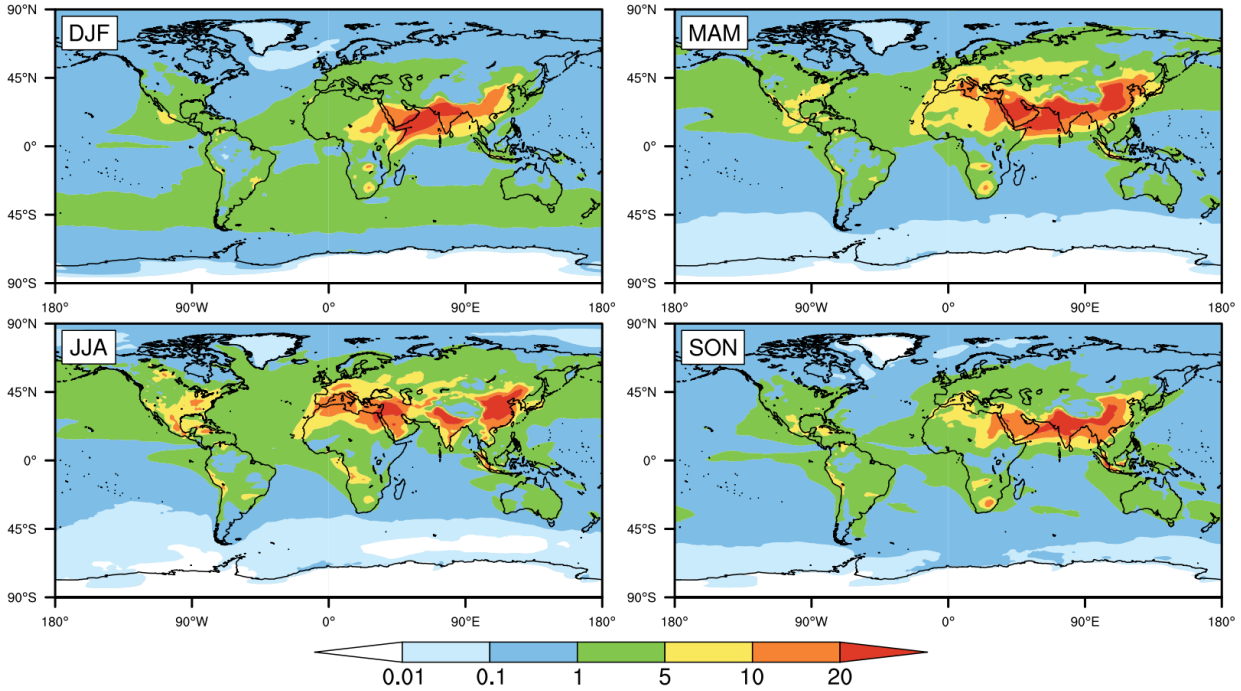

Figure 2. Global distribution of seasonally averaged surface concentrations of sulfate (unit: $\mu g \cdot m^{-3}$) in 2015, simulated by CESM2 with standard configuration (i.e., the Original case). DJF, MAM, JJA and SON represent December-January-February, March-April-May, June-July-August and September-October-November, respectively, which is the same below.

After incorporating the detailed in-cloud aqueous-phase chemical mechanisms and enhancing the WD rate of sulfate, the concentrations of sulfate dropped markedly in all seasons, as shown in Figure 3. In general, the reductions in sulfate do not exceed 5 $\mu g \cdot m^{-3}$ in most regions, especially over the ocean. In some regions, such as EA, SA and ME, the sulfate concentrations can still decrease by more than 10 $\mu g \cdot m^{-3}$. This distribution is high, corresponding to that of the simulated background sulfate concentrations shown in Figure 2. Similarly, there are no distinct seasonal differences in sulfate reduction. The reduction in spring and summer is only slightly more significant than that in autumn and winter.

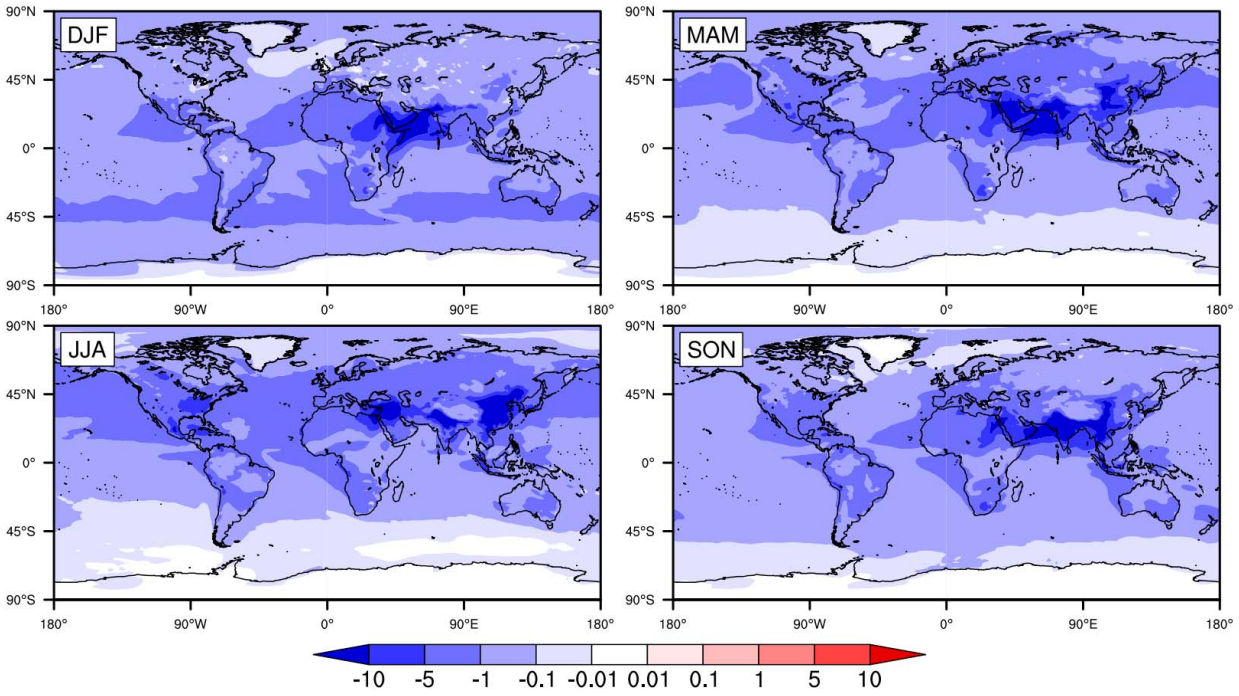

Figure 3. The differences in global seasonally averaged surface sulfate concentrations (unit: $\mu g \cdot m^{-3}$) between the Improved case and the Original case in 2015 after incorporation of detailed in-cloud aqueous-phase chemical mechanisms and enhanced wet deposition flux of sulfate (i.e., Case 6 minus Case 1).

3.2 Comparison between the simulated and observed surface sulfate concentrations

A comparison with the observations of sulfate in different regions exhibits the accuracy of the model simulation of sulfate. Figure 4 shows the observed and simulated monthly average surface sulfate concentrations in the three monitoring networks over the EU (EMEP), NAM (IMPROVE) and Asia (EANET). The observations from the EANET monitoring network are further divided into “Japan and South Korea” and “Other Asia countries”, as shown in Figure S1. First, the observed concentrations of sulfate in all three regions mentioned above are relatively consistent throughout the year without large fluctuations. Compared with the observations, it is noteworthy that the surface sulfate concentrations in the Original simulation are severely overestimated in all three regions and in almost all months, especially from April to September.

The coupling of detailed in-cloud aqueous-phase chemical mechanisms enhances the oxidation capacity of SO_2 and further increases the sulfate concentration, especially in autumn and winter in EU and NAM and throughout the year in AS. As indicated in Ge et al. (2021), the coupling of detailed in-cloud chemistry significantly lowers SO_2 concentrations and fits well with the observations. However, this results in a larger overestimation of sulfate. After adjusting the WD flux of sulfate, the concentrations decreased considerably in nearly all months. The greater the WD flux is, the lower the sulfate concentration is. Notably, the sulfate concentrations drop the most significantly at 5 times the Original WD flux and show a small, further decrease when switching to 10 or 20 times the Original WD flux. Regardless of the region, the simulations show remarkable improvement, and nearly all the Improved surface sulfate concentrations are within the range of the standard deviation of the observations, with the exception of summer in the EU. The notable overestimates in the EU in July and August may be related to the Mediterranean climate with insufficient precipitation in summer in parts of the EU, leading to the limited effect of sulfate WD.

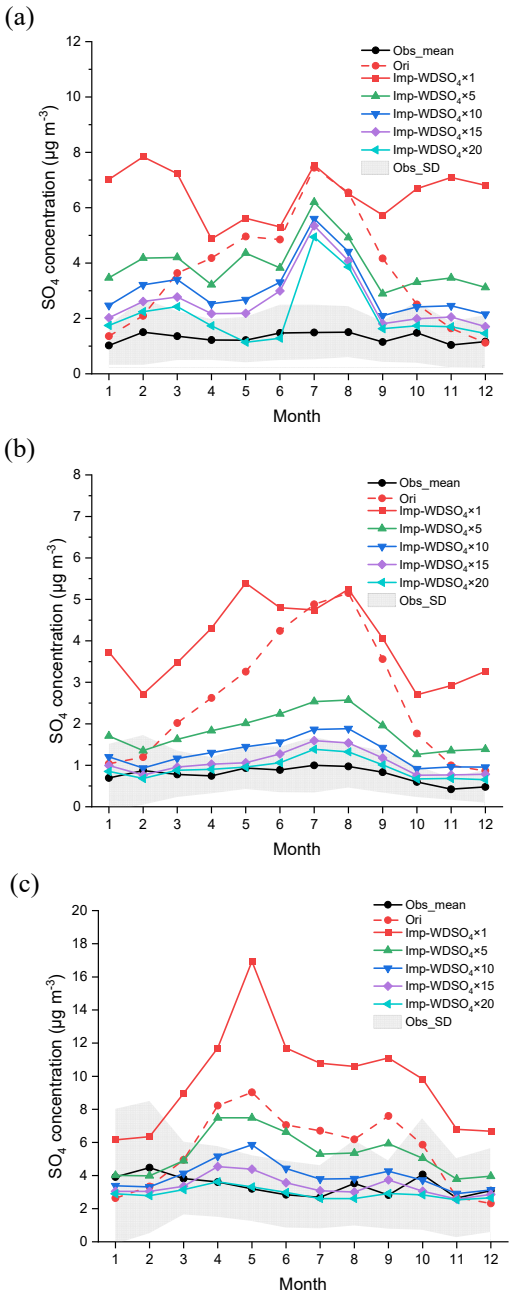

Figure 4. Monthly average surface sulfate concentrations (μg·m^{-3}) in EU, NAM, and Asia in 2015. The black solid lines and red dashed lines represent the observed and Original simulated concentrations, respectively. Other lines represent improved sulfate concentrations with different levels of sulfate wet deposition fluxes. The multiples of sulfate wet deposition from top to bottom are 1, 5, 10, 15 and 20 (i.e., the Improved case). The gray areas represent the standard deviation of the observed concentrations. The observed concentrations are calculated by averaging the data from all monitoring stations over a region. The simulated

concentrations are calculated by averaging the data from all the grids where the monitoring stations are located. The corresponding monitoring networks are (a) EMEP, (b) IMPROVE and (c) EANET.

3.3 Comparison between the simulated and aircraft observations

In addition to surface concentrations, sulfates at higher altitudes are also very important in terms of their climate effects on clouds and radiation and are thus compared with various aircraft measurements (see Figures 5 and S2). First, regardless of the aircraft measurement or simulation case, the distribution of sulfate concentration changes substantially with height (from more than 10 $\mu g \cdot m^{-3}$ near the surface to near 0 $\mu g \cdot m^{-3}$ at higher altitudes). Overall, the sulfate is concentrated near the ground and decreases with increasing height. Similar to the results of the surface sulfate concentration, when compared with the aircraft observations, the results of the Original case are notably overestimated, especially at low altitudes and near the ground. The coupling of in-cloud aqueous-phase mechanisms still further increases the sulfate concentration to some extent. After enhancing the WD flux, sulfate concentrations decrease markedly. The declining characteristics with different multiples are basically consistent with the surface sulfate results. That is, the higher the multiple is, the lower the concentration is and the smaller the decrease range is. Finally, most of the Improved sulfate concentrations at different altitudes are within the range of the standard deviation of aircraft observations. The overestimation of sulfate concentrations at low altitudes has been greatly mitigated.

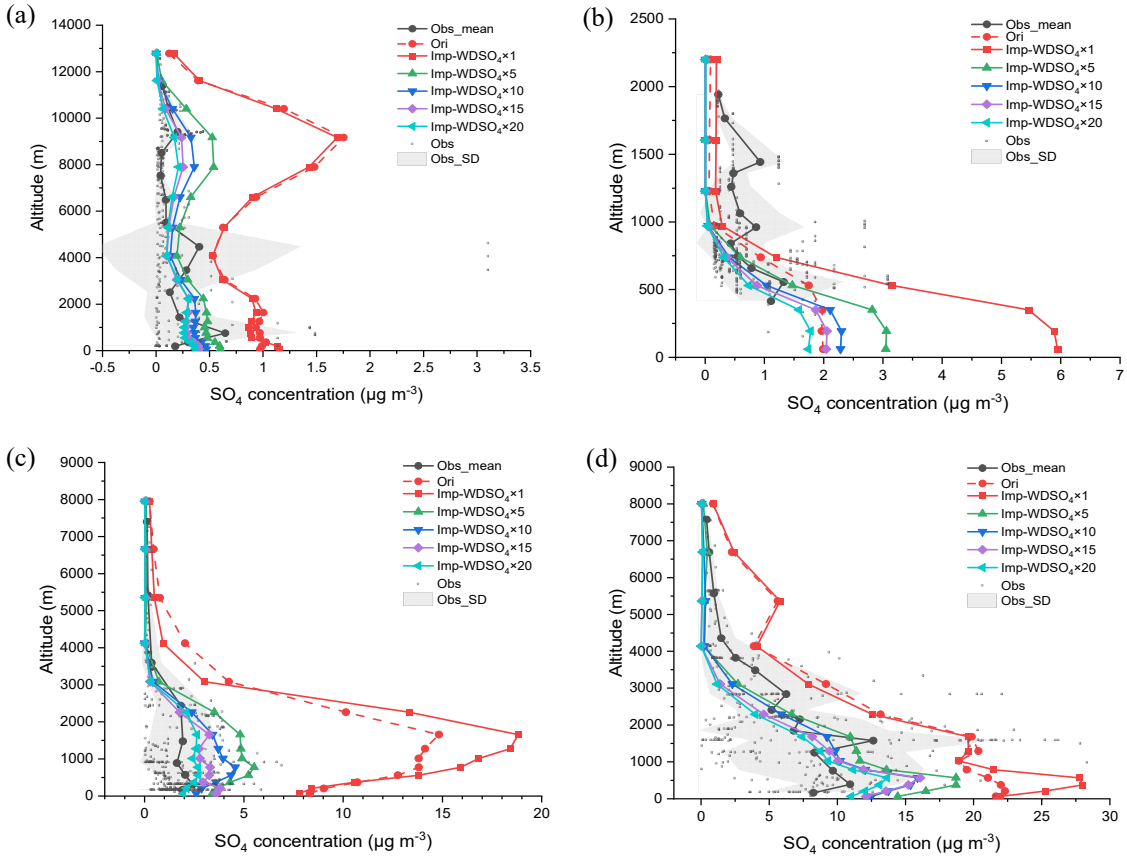

Figure 5. Vertical profiles of sulfate concentrations (μg·m^{-3}) over different regions. The black solid lines represent the average observed concentrations at different altitudes. The red dashed lines represent the Original simulated concentrations on the same day in 2015. Other lines represent improved sulfate concentrations with different levels of sulfate wet deposition fluxes. The multiples of sulfate wet deposition from top to bottom are 1, 5, 10, 15 and 20 (i.e., the Improved case). The gray areas represent the standard deviation of the observed concentrations. The black dots represent every single observational data point. The corresponding aircraft measurement campaigns are (a) ATom on 15 August 2016, (b) WINTER on 3 March 2015 and (c-d) KORUS-AQ on 10 May 2016 and 30 May 2016.

Nevertheless, the sulfate concentrations at high altitudes are underestimated in some cases. Therefore, lines of the observed and simulated results generally meet at the boundary layer height (overestimate at lower levels and underestimate at higher levels), ranging from 1 to 4 km, as shown in Figures 5 and S2 (Kipling et al., 2016). All the deviations in the sulfate concentration simulation at different altitudes and the variability in cross regions may lead to great uncertainty in the subsequent assessment of the RF of sulfate. Therefore, we performed a series of sensitivity tests on RF in section 5.

In summary, the incorporation of in-cloud aqueous-phase mechanisms and an increase in sulfate WD greatly decreases the concentration and mitigates the deviation in the sulfate simulation, thus significantly improving the overall performance of sulfate simulation both near the ground and at high altitudes.

4 Global radiative forcing from the sulfate distribution

4.1 Radiative forcing of sulfate in different sensitivity simulations

Sulfate has a cooling effect on climate. Therefore, the substantial reduction in simulated sulfate concentrations after improvement will elevate its RF (Figure 6). Clearly, the RF of sulfate increases evidently in all seasons and nearly all regions worldwide, which means an improved global sulfate distribution may weaken its cooling effect significantly. Similar to the results in Figures 2 and 3, such an increase in RF is also distributed unevenly throughout the world, mainly in EA, SA, ME, EU and in low- and middle-latitude regions, where the value usually exceeds 5 W·m^{-2}. Most high-latitude regions are rarely affected, and the increase is no more than 0.5 W·m^{-2}, which is in accordance with the relatively low background distribution of the sulfate concentration. Although the increase is greater in spring and summer to some extent, the fluctuation is not intense throughout the year. Overall, the incorporation of in-cloud aqueous-

phase mechanisms and an increase in sulfate WD lead to lower SO_2/sulfate concentrations and a smaller cooling effect of sulfate, as shown in Figures 7 and S3.

4.2 Radiative forcing of global anthropogenic sulfate

The incorporation of in-cloud aqueous-phase mechanisms and an increase in sulfate WD could affect the simulation of sulfate RF from anthropogenic emissions since 1750. The RF of sulfate in 2011 relative to 1750 (-0.41 $W \cdot m^{-2}$, -0.62 to -0.21 $W \cdot m^{-2}$) was provided in the fifth report of IPCC (Intergovernmental Panel on Climate, 2014), as shown in Figure 7. We also referred to and summarized several previous studies related to the assessment of sulfate RF in Figure 7. Moreover, the results of our Original and Improved simulations of sulfate RF in 2015 relative to 1850 are also shown in Figures 7 and S3. We also simulated the corresponding two RFs of all anthropogenic sulfates by complete removal of all anthropogenic emissions (i.e., Original and Improved anthro-removed simulations). Compared with the results of the IPCC report, it is obvious that the RF of sulfate in the Original simulations is severely overestimated. The incorporation of in-cloud aqueous-phase mechanisms and an increase in sulfate WD markedly reduce the overestimation. The corresponding two improved-simulated RFs are -0.382 and -0.410 $W \cdot m^{-2}$, which are comparable to the IPCC report and other, previous studies (Chuang, Penner, Taylor, Grossman, & Walton, 1997; Haywood & Ramaswamy, 1998; B. Li et al., 2018; X. Ma, Shi, Guo, & Wang, 2005; Matus, L'Ecuyer, & Henderson, 2019; Ni, Zheng, Ma, Wang, & Wang, 2016; Penner, Chuang, & Grant, 1998).

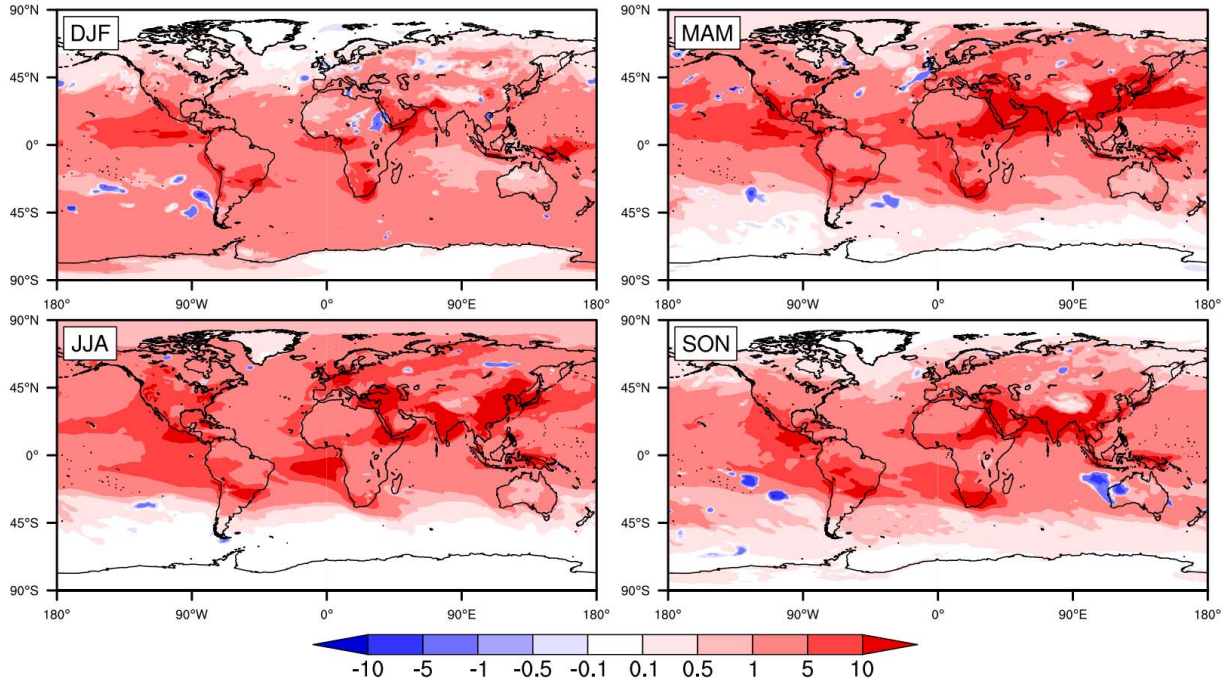

Figure 6. The differences in global seasonally averaged sulfate radiative forcing (unit: $W \cdot m^{-2}$) between the Improved case and the Original case in 2015 after the incorporation of

detailed in-cloud aqueous-phase chemical mechanisms and multiplication of the wet deposition flux of sulfate.

The results indicate that the current model tends to overestimate the sulfate concentration, which in turn leads to overestimation of the negative RF and cooling effect of sulfate. After the incorporation of in-cloud aqueous-phase mechanisms and enhancement of sulfate WD, the simulations could significantly mitigate the deviation in the concentration and RF assessments of sulfate. Such improvements could also verify the reliability of the IPCC report.

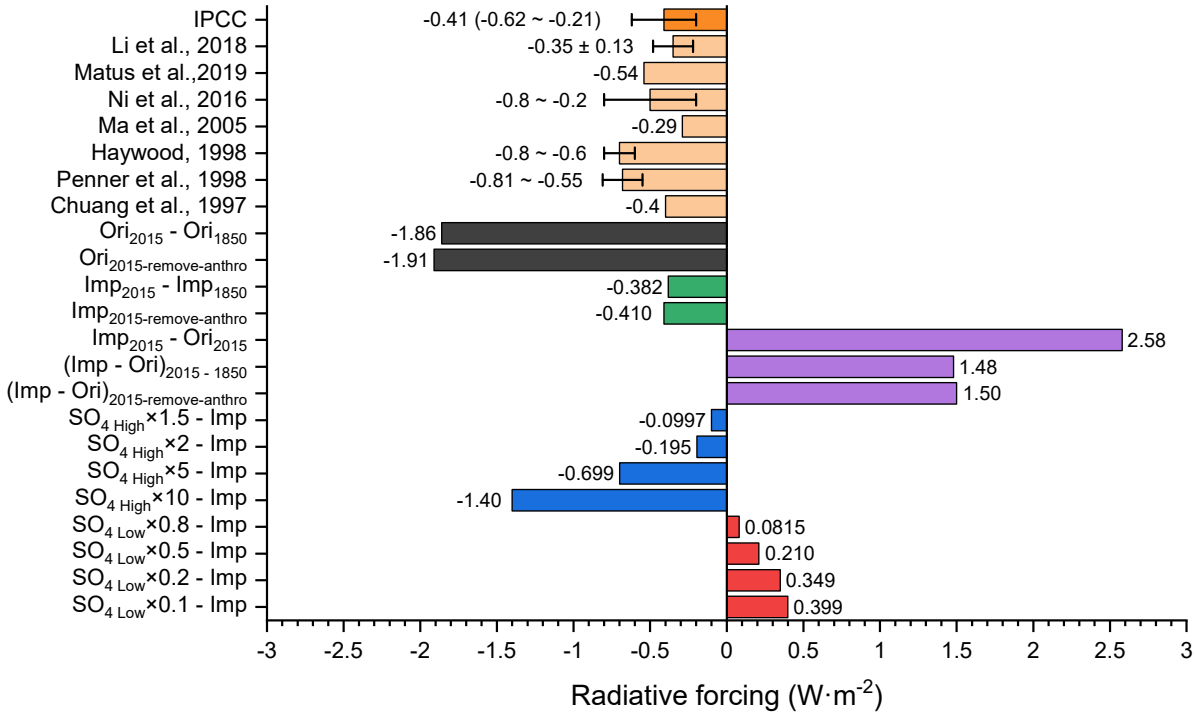

Figure 7. Radiative forcing of sulfate in different simulation cases and references (Chuang et al., 1997; Haywood & Ramaswamy, 1998; Intergovernmental Panel on Climate, 2014; B. Li et al., 2018; X. Ma et al., 2005; Matus et al., 2019; Ni et al., 2016; Penner et al., 1998).

5 Factors influencing the simulation of sulfate radiative forcing and uncertainty analysis

Model evaluation shows an underestimation of sulfate concentration at high altitudes but overestimation within the boundary layer (shown in sections 3.2 and 3.3). This finding would lead to great uncertainty in the estimate of sulfate RF. To understand the potential variability in sulfate RF, we conducted additional sensitivity tests, as shown in Figure 8. To better fit the simulated sulfate concentration with the aircraft observations, we enhance sulfate concentrations by factors of 1~10 above the boundary layer and reduce boundary layer sulfate concentrations by factors of 1~0.1. The demarcation height of these two uncertainty factors is set to 2.0 km, and

four additional levels (1.2, 1.5, 2.7, and 3.6 km) were also added given the range of this value from 1 to 4 km in section 3.3.

Figure 8 shows the differences in sulfate RF between all the sensitivity tests and the Improved case. The corresponding global annual distributions are shown in Figures S4-5. The RF values in Figure 8a increase from left to right, indicating that the decrease in sulfate concentration at low altitude leads to weakening of the cooling effect of sulfate and increases the RF values from the Improved case. The maximum difference value is +0.399 $W \cdot m^{-2}$ when the sulfate concentration below 2.0 km is reduced by 90%, as shown in Figure 7. On the other hand, the values decrease from bottom to top, indicating that the increase in sulfate concentration at high altitudes strengthens the cooling effect of sulfate and results in negative RF values. Similarly, when the sulfate concentration above 2.0 km increases by a factor of 10, the RF value is reduced by 1.40 $W \cdot m^{-2}$ from the Improved case.

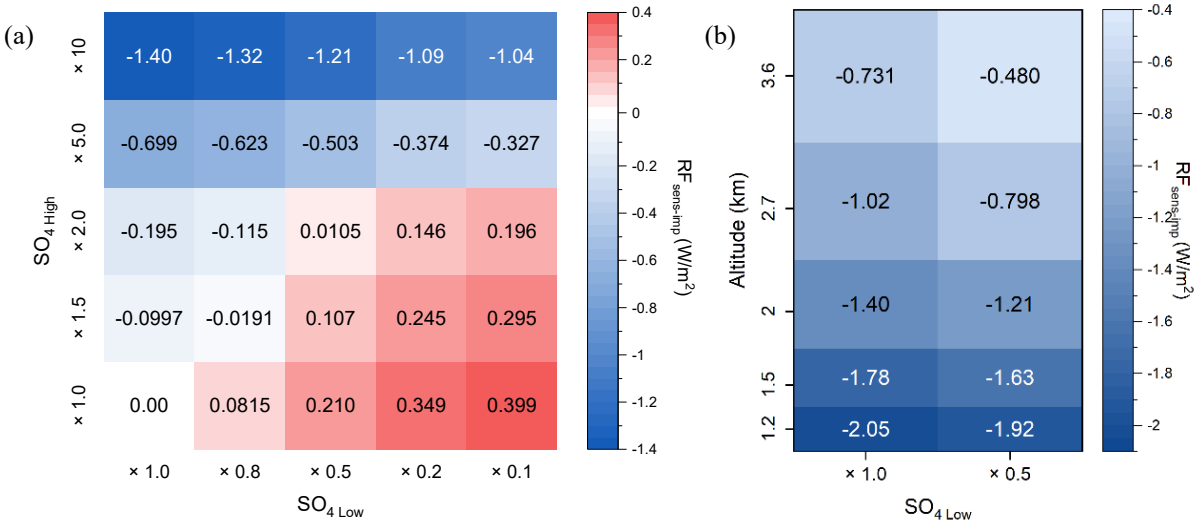

Figure 8. The differences in annual global-mean sulfate radiative forcing (unit: $W \cdot m^{-2}$) between each sensitivity test and the Improved case in 2015. (a) The horizontal direction is the sensitivity test for decreasing the sulfate concentration at low altitude (below 2.0 km). The decrease factors from left to right are 1.0, 0.8, 0.5, 0.2, and 0.1, indicating that the sulfate concentrations below 2.0 km are 100%, 80%, 50%, 20% and 10% of the Improved case, respectively. The vertical direction is the sensitivity test for increasing the sulfate concentration at high altitudes (above 2.0 km). The increase factors from bottom to top are 1.0, 1.5, 2.0, 5.0, and 10. (b) The vertical direction is the sensitivity test of changing the altitude of the turning point (TP, the altitude above which the model tends to

underestimate sulfate concentrations and below which the model tends to overestimate sulfate concentrations). The altitudes of the TP are set from bottom to top as 1.2, 1.5, 2.0, 2.7, and 3.6 km. The decreasing factors for sulfate concentration at low altitude are 1.0 and 0.5, and the increasing factor for sulfate concentration at high altitude is 10.

Notably, the sulfate RF basically shows a linear trend with its concentration. At the same time, the differences between the bundles "1.0×1.0" (0 $W \cdot m^{-2}$) and "2.0×1.0" (-0.195 $W \cdot m^{-2}$) is -0.195 $W \cdot m^{-2}$, indicating that the RF was contributed by sulfate above 2.0 km. Then, according to the maximum (+0.399 $W \cdot m^{-2}$) above, we can roughly estimate that the ratio of sulfate content between "< 2.0 km" and ">2.0 km" is 2.2:1, which means that most sulfate is concentrated near the ground. In addition, from the two RFs above, we can generally determine that the total RF of sulfate, including anthropogenic and natural sources, is 0.63 $W \cdot m^{-2}$. Then, compared with the RF of anthropogenic sulfate only (-0.410 $W \cdot m^{-2}$) shown in Figure 7, we could also roughly estimate that the RF of natural sulfate is approximately -0.22 $W \cdot m^{-2}$, and the ratio between anthropogenic and natural sulfate RF is approximately 1.8:1, which means that natural sources from the ocean (e.g., DMS) contribute approximately one-third of sulfate RF, and anthropogenic emissions account for the remaining two-thirds.

In conclusion, the overestimation of the sulfate concentration near the ground would in turn overestimate its cooling effect to some extent. The removal of excess sulfate would lessen the negative RF of sulfate. In contrast, the underestimation of sulfate at high altitudes would further lead to the underestimation of sulfate RF. The supplement for such underestimation will significantly increase the negative RF of sulfate, which indicates that the underestimated sulfate at high altitudes in the simulation has a much stronger cooling potential. Therefore, the overestimation or underestimation of sulfate concentrations at different heights will significantly increase the deviation and uncertainty of the evaluation of sulfate RF.

Finally, with regard to the sensitivity tests of changing the TP altitude, Figure 8b shows that whether the decrease factors at low altitude are 1.0 or 0.5, the negative sulfate RF increases with the decrease in TP. The downward movement of the TP enlarges the high-altitude area where the model underestimates sulfate concentrations and therefore increases the negative RF of sulfate. When the TP drops to 1.2 km, the sulfate RF can be further decreased by up to 2.05 $W \cdot m^{-2}$ based on the Improved-simulation. The opposite is true when elevating the TP altitude, which expands the low-altitude area and weakens the cooling effect of sulfate. Furthermore, it should be noted that various aircraft observations in section 3.3 involve different time periods throughout the year and different regions around the world. This understanding infers a much broader fluctuation of the TP altitudes when comparing the simulated and observed sulfate concentrations at annual and global scales, which might also bring substantial uncertainties to the evaluation of sulfate RF.

Based on the analysis above, although the improved RF of sulfate estimated in this study is close to that of the IPCC report, there is the potential that the true sulfate RF may deviate significantly from either this study or the IPCC report. This deviation may partly come from the

uncertainty of emission inventories, sulfur chemistry and sulfate wet deposition during model simulations. Therefore, it is necessary to update relevant emission data in a timely manner and strengthen the field study of sulfate in terms of its concentrations and wet deposition at different altitudes and regions and seasons to mitigate the uncertainty of sulfate RF and provide a more reliable assessment of climate change.

6 Conclusions and discussion

In view of the uncertainty of global simulation of sulfate concentration and the related RF, this study used CESM2 and PORT models to evaluate and improve their simulation performance of sulfate. After the incorporation of detailed in-cloud aqueous-phase chemical mechanisms and enhanced wet deposition flux of sulfate, the simulation of sulfate concentration improved significantly both near the ground and at high altitude compared with observations. Consequently, such improvement in simulations of sulfate distribution further improved the simulation of sulfate RF. The Improved-simulated RFs of sulfate from 1850 to 2015 and all anthropogenic sources are -0.382 and -0.410 $W \cdot m^{-2}$, respectively, which are both comparable to the IPCC report and other, previous studies. Our results indicated that the wet deposition of sulfate is one of the important sources of uncertainty in its concentration simulation. Furthermore, the surface overestimation and high-altitude underestimation of sulfate are the main uncertainty factors of the sulfate RF simulation. As reported in IPCC AR5 and 6, aerosols partially offset the RF of well-mixed greenhouse gases, which is the most uncertain part of the total anthropogenic forcing in climate change (Intergovernmental Panel on Climate, 2014; B. Li et al., 2018; H. Zhang & Huang, 2014). As an important component of aerosols and sources of negative forcing, sulfate, with its wet scavenging and related cloud processes, remains a key source of uncertainty in the estimation of global RF.

Many countries and regions (e.g., EU, US, Japan and China) have focused more attention and efforts on air pollution control in recent years, and the emissions and concentrations of PM and sulfate in the atmosphere have decreased rapidly (Aas et al., 2019; Attwood et al., 2014; Breider et al., 2017; Dai et al., 2021; J. Feng et al., 2021; Karplus, Zhang, & Almond, 2018; Rogora, Colombo, Marchetto, Mosello, & Steingruber, 2016; Yan & Xu, 2021). Therefore, the emission data sources need to be updated promptly. Moreover, it is worth emphasizing that since the lifetime of sulfate is relatively short compared with that of CO_2, the climate response from sulfate emission changes may happen at a much faster pace than CO_2. If global models underestimate the sulfate cooling effects at high altitudes, they could already counteract the warming effect of CO_2 significantly. As an increasing number of countries set carbon neutral targets for the near future and rapidly phase out the use of fossil energy, anthropogenic sulfur emissions will decline accordingly, which may cause a much more intensive warming effect than expected in the short term, especially in China. Notably, various policies aiming to reduce pollution over China have resulted in a dramatic decrease in aerosols, causing in an overall warming effect due to the dominant role of sulfate reductions in the period of 2012~2021 (Bae, Kim, Kim, Kim, & Kim, 2021; Fioletov et al., 2016; Geng et al., 2019; Jo et al., 2020; X. Li et al., 2020). “Carbon peaking” and “carbon neutrality” goals were first announced in 2020 in China. Consequently, the energy and industrial structures of these regions are bound to transform gradually in the future, followed by remarkable changes in the emissions and levels of various pollutants, including sulfate. Therefore, it is of great importance to estimate the RF of short-lived

518 pollutants and its contribution to global climate change in the following decades. All these issues
519 will be examined in our future work.

520 **Acknowledgments**

521 This work was supported by funding from the National Natural Science Foundation of China
522 (under award nos. 41821005, 42077196). The authors declare that they have no conflict of
523 interest.

524 **Open Research**

525 The Community Earth System Model 2 (CESM2) developed by the National Center for Atmospheric
526 Research can be downloaded online (https://www.cesm.ucar.edu/models/cesm2/). All codes used to
527 generate the results of this study are available from the authors upon request. The CMIP6 emission
528 datasets analyzed during the current study are available at https://svn-ccsm-
529 inputdata.cgd.ucar.edu/trunk/inputdata/atm/cam/chem/. The MERRA2 meteorological offline data
530 are publicly available from https://rda.ucar.edu/datasets/ds313.3/.

531

532

533 **References**

534 Aas, W., Mortier, A., Bowersox, V., Cherian, R., Faluvegi, G., Fagerli, H., . . . Xu, X. (2019).
535 Global and regional trends of atmospheric sulfur. *Scientific Reports, 9*. doi:10.1038/s41598-018-
536 37304-0

537 Asutosh, A., Fadnavis, S., Nuncio, M., Mueller, R., & Tripathy, S. C. (2021). The Arctic
538 Temperature Response to Global and Regional Anthropogenic Sulfate Aerosols. *Frontiers in*
539 *Environmental Science, 9*. doi:10.3389/fenvs.2021.766538

540 Attwood, A. R., Washenfelder, R. A., Brock, C. A., Hu, W., Baumann, K., Campuzano-Jost, P., .
541 . . Brown, S. S. (2014). Trends in sulfate and organic aerosol mass in the Southeast U.S.: Impact

on aerosol optical depth and radiative forcing. *Geophysical Research Letters, 41*(21), 7701-7709. doi:10.1002/2014gl061669

Aubry, T. J., Staunton-Sykes, J., Marshall, L. R., Haywood, J., Abraham, N. L., & Schmidt, A. (2021). Climate change modulates the stratospheric volcanic sulfate aerosol lifecycle and radiative forcing from tropical eruptions. *Nature Communications, 12*(1). doi:10.1038/s41467-021-24943-7

Bae, M., Kim, B.-U., Kim, H. C., Kim, J., & Kim, S. (2021). Role of emissions and meteorology in the recent $PM_{2.5}$ changes in China and South Korea from 2015 to 2018. *Environmental Pollution, 270*. doi:10.1016/j.envpol.2020.116233

Breider, T. J., Mickley, L. J., Jacob, D. J., Ge, C., Wang, J., Sulprizio, M. P., . . . Hopke, P. K. (2017). Multidecadal trends in aerosol radiative forcing over the Arctic: Contribution of changes in anthropogenic aerosol to Arctic warming since 1980. *Journal of Geophysical Research-Atmospheres, 122*(6), 3573-3594. doi:10.1002/2016jd025321

Buchard, V., da Silva, A. M., Colarco, P., Krotkov, N., Dickerson, R. R., Stehr, J. W., . . . He, H. (2014). Evaluation of GEOS-5 sulfur dioxide simulations during the Frostburg, MD 2010 field campaign. *Atmospheric Chemistry and Physics, 14*(4), 1929-1941. doi:10.5194/acp-14-1929-2014

Carslaw, K. S., Gordon, H., Hamilton, D. S., Johnson, J. S., Regayre, L. A., Yoshioka, M., & Pringle, K. J. (2017). Aerosols in the Pre-industrial Atmosphere. *Current Climate Change Reports, 3*(1), 1-15. doi:10.1007/s40641-017-0061-2

Chen, C.-C., & Gettelman, A. (2016). Simulated 2050 aviation radiative forcing from contrails and aerosols. *Atmospheric Chemistry and Physics, 16*(11), 7317-7333. doi:10.5194/acp-16-7317-2016

565 Chen, Z., Huang, T., Huang, X., Han, X., Yang, H., Cai, Z., . . . Huang, C. (2019).
566 Characteristics, sources and environmental implications of atmospheric wet nitrogen and sulfur
567 deposition in Yangtze River Delta. *Atmospheric Environment, 219*.
568 doi:10.1016/j.atmosenv.2019.116904
569 Cheng, Y., Zheng, G., Wei, C., Mu, Q., Zheng, B., Wang, Z., . . . Su, H. (2016). Reactive
570 nitrogen chemistry in aerosol water as a source of sulfate during haze events in China. *Science*
571 *Advances, 2*(12). doi:10.1126/sciadv.1601530
572 Chuang, C. C., Penner, J. E., Taylor, K. E., Grossman, A. S., & Walton, J. J. (1997). An
573 assessment of the radiative effects of anthropogenic sulfate. *Journal of Geophysical Research-*
574 *Atmospheres, 102*(D3), 3761-3778. doi:10.1029/96jd03087
575 Conley, A. J., Lamarque, J. F., Vitt, F., Collins, W. D., & Kiehl, J. (2013). PORT, a CESM tool
576 for the diagnosis of radiative forcing. *Geoscientific Model Development, 6*(2), 469-476.
577 doi:10.5194/gmd-6-469-2013
578 Conradie, E. H., Van Zyl, P. G., Pienaar, J. J., Beukes, J. P., Galy-Lacaux, C., Venter, A. D., &
579 Mkhatshwa, G. V. (2016). The chemical composition and fluxes of atmospheric wet deposition
580 at four sites in South Africa. *Atmospheric Environment, 146*, 113-131.
581 doi:10.1016/j.atmosenv.2016.07.033
582 Cziczo, D. J., Froyd, K. D., Hoose, C., Jensen, E. J., Diao, M., Zondlo, M. A., . . . Murphy, D.
583 M. (2013). Clarifying the Dominant Sources and Mechanisms of Cirrus Cloud Formation.
584 *Science, 340*(6138), 1320-1324. doi:10.1126/science.1234145
585 Dai, T., Cheng, Y., Goto, D., Li, Y., Tang, X., Shi, G., & Nakajima, T. (2021). Revealing the
586 sulfur dioxide emission reductions in China by assimilating surface observations in WRF-Chem.
587 *Atmospheric Chemistry and Physics, 21*(6), 4357-4379. doi:10.5194/acp-21-4357-2021

588 Danabasoglu, G., Lamarque, J. F., Bacmeister, J., Bailey, D. A., DuVivier, A. K., Edwards, J., . .
589 . Strand, W. G. (2020). The Community Earth System Model Version 2 (CESM2). *Journal of*
590 *Advances in Modeling Earth Systems, 12*(2), 1-35. doi:10.1029/2019ms001916
591 de Meij, A., Krol, M., Dentener, F., Vignati, E., Cuvelier, C., & Thunis, P. (2006). The
592 sensitivity of aerosol in Europe to two different emission inventories and temporal distribution of
593 emissions. *Atmospheric Chemistry and Physics, 6*, 4287-4309. doi:10.5194/acp-6-4287-2006
594 Dentener, F., Drevet, J., Lamarque, J. F., Bey, I., Eickhout, B., Fiore, A. M., . . . Wild, O. (2006).
595 Nitrogen and sulfur deposition on regional and global scales: A multimodel evaluation. *Global*
596 *Biogeochemical Cycles, 20*(4). doi:10.1029/2005gb002672
597 Driscoll, C. T., Driscoll, K. M., Fakhraei, H., & Civerolo, K. (2016). Long-term temporal trends
598 and spatial patterns in the acid-base chemistry of lakes in the Adirondack region of New York in
599 response to decreases in acidic deposition. *Atmospheric Environment, 146*, 5-14.
600 doi:10.1016/j.atmosenv.2016.08.034
601 Echeverria, M., Abreu, C. M., Gonzalez, A., Ortega, A., & Echeverria, C. A. (2016). Towards
602 the Determination of the Origin of Sulfur Compounds in Marine Zones by Means of the
603 Chloride/Sulfate Ratio: Applications in Atmospheric Corrosion Studies. *Journal of the*
604 *Electrochemical Society, 163*(6), C316-C323. doi:10.1149/2.0751606jes
605 Emmons, L. K., Schwantes, R. H., Orlando, J. J., Tyndall, G., Kinnison, D., Lamarque, J. F., . . .
606 Pétron, G. (2020). The Chemistry Mechanism in the Community Earth System Model Version 2
607 (CESM2). *Journal of Advances in Modeling Earth Systems, 12*(4), 1-21.
608 doi:10.1029/2019ms001882
609 Emmons, L. K., Walters, S., Hess, P. G., Lamarque, J. F., Pfister, G. G., Fillmore, D., . . .
610 Kloster, S. (2010). Description and evaluation of the Model for Ozone and Related chemical

611 Tracers, version 4 (MOZART-4). *Geoscientific Model Development, 3*(1), 43-67.
612 doi:10.5194/gmd-3-43-2010

613 Faloona, I. (2009). Sulfur processing in the marine atmospheric boundary layer: A review and
614 critical assessment of modeling uncertainties. *Atmospheric Environment, 43*(18), 2841-2854.
615 doi:10.1016/j.atmosenv.2009.02.043

616 Fedkin, N. M., Li, C., Dickerson, R. R., Canty, T., & Krotkov, N. A. (2019). Linking
617 improvements in sulfur dioxide emissions to decreasing sulfate wet deposition by combining
618 satellite and surface observations with trajectory analysis. *Atmospheric Environment, 199*, 210-
619 223. doi:10.1016/j.atmosenv.2018.11.039

620 Feng, J., Vet, R., Cole, A., Zhang, L., Cheng, I., O'Brien, J., & Macdonald, A.-M. (2021).
621 Inorganic chemical components in precipitation in the eastern US and Eastern Canada during
622 1989-2016: Temporal and regional trends of wet concentration and wet deposition from the
623 NADP and CAPMoN measurements. *Atmospheric Environment, 254*.
624 doi:10.1016/j.atmosenv.2021.118367

625 Feng, L., Smith, S. J., Braun, C., Crippa, M., Gidden, M. J., Hoesly, R., . . . van der Werf, G. R.
626 (2020). The generation of gridded emissions data for CMIP6. *Geoscientific Model Development,*
627 *13*(2), 461-482. doi:10.5194/gmd-13-461-2020

628 Fioletov, V. E., McLinden, C. A., Krotkov, N., Li, C., Joiner, J., Theys, N., . . . Moran, M. D.
629 (2016). A global catalogue of large SO_2 sources and emissions derived from the Ozone
630 Monitoring Instrument. *Atmospheric Chemistry and Physics, 16*(18), 11497-11519.
631 doi:10.5194/acp-16-11497-2016

Flanner, M. G., Gardner, A. S., Eckhardt, S., Stohl, A., & Perket, J. (2014). Aerosol radiative forcing from the 2010 Eyjafjallajokull volcanic eruptions. *Journal of Geophysical Research-Atmospheres, 119*(15), 9481-9491. doi:10.1002/2014jd021977

Gao, M., Carmichael, G. R., Wang, Y., Ji, D., Liu, Z., & Wang, Z. (2016). Improving simulations of sulfate aerosols during winter haze over Northern China: the impacts of heterogeneous oxidation by NO_2. *Frontiers of Environmental Science & Engineering, 10*(5). doi:10.1007/s11783-016-0878-2

Ge, W., Liu, J., Yi, K., Xu, J., Zhang, Y., Hu, X., . . . Tao, S. (2021). Influence of atmospheric in-cloud aqueous-phase chemistry on the global simulation of SO_2 in CESM2. *Atmos. Chem. Phys., 21*(21), 16093-16120. doi:10.5194/acp-21-16093-2021

Gelaro, R., McCarty, W., Suarez, M. J., Todling, R., Molod, A., Takacs, L., . . . Zhao, B. (2017). The Modern-Era Retrospective Analysis for Research and Applications, Version 2 (MERRA-2). *Journal of Climate, 30*(14), 5419-5454. doi:10.1175/jcli-d-16-0758.1

Geng, G., Xiao, Q., Zheng, Y., Tong, D., Zhang, Y., Zhang, X., . . . Liu, Y. (2019). Impact of China's Air Pollution Prevention and Control Action Plan on $PM_{2.5}$ chemical composition over eastern China. *Science China-Earth Sciences, 62*(12), 1872-1884. doi:10.1007/s11430-018-9353-x

Georgiou, G. K., Christoudias, T., Proestos, Y., Kushta, J., Hadjinicolaou, P., & Lelieveld, J. (2018). Air quality modelling in the summer over the eastern Mediterranean using WRF-Chem: chemistry and aerosol mechanism intercomparison. *Atmospheric Chemistry and Physics, 18*(3), 1555-1571. doi:10.5194/acp-18-1555-2018

653 Goto, D., Nakajima, T., Takemura, T., & Sudo, K. (2011). A study of uncertainties in the sulfate
654 distribution and its radiative forcing associated with sulfur chemistry in a global aerosol model.
655 *Atmospheric Chemistry and Physics, 11*(21), 10889-10910. doi:10.5194/acp-11-10889-2011
656 Green, J. R., Fiddler, M. N., Holloway, J. S., Fibiger, D. L., McDuffie, E. E., Campuzano-Jost,
657 P., . . . Brown, S. S. (2019). Rates of Wintertime Atmospheric SO_2 Oxidation based on Aircraft
658 Observations during Clear-Sky Conditions over the Eastern United States. *Journal of*
659 *Geophysical Research-Atmospheres, 124*(12), 6630-6649. doi:10.1029/2018jd030086
660 Haywood, J. M., & Ramaswamy, V. (1998). Global sensitivity studies of the direct radiative
661 forcing due to anthropogenic sulfate and black carbon aerosols. *Journal of Geophysical*
662 *Research-Atmospheres, 103*(D6), 6043-6058. doi:10.1029/97jd03426
663 Hoesly, R. M., Smith, S. J., Feng, L., Klimont, Z., Janssens-Maenhout, G., Pitkanen, T., . . .
664 Zhang, Q. (2018). Historical (1750-2014) anthropogenic emissions of reactive gases and aerosols
665 from the Community Emissions Data System (CEDS). *Geoscientific Model Development, 11*(1),
666 369-408. doi:10.5194/gmd-11-369-2018
667 Horowitz, L. W. (2006). Past, present, and future concentrations of tropospheric ozone and
668 aerosols: Methodology, ozone evaluation, and sensitivity to aerosol wet removal. *Journal of*
669 *Geophysical Research-Atmospheres, 111*(D22). doi:10.1029/2005jd006937
670 Huang, L., An, J., Koo, B., Yarwood, G., Yan, R., Wang, Y., . . . Li, L. (2019). Sulfate formation
671 during heavy winter haze events and the potential contribution from heterogeneous SO_2 + NO_2
672 reactions in the Yangtze River Delta region, China. *Atmospheric Chemistry and Physics, 19*(22),
673 14311-14328. doi:10.5194/acp-19-14311-2019

674 Huang, X., Song, Y., Zhao, C., Li, M., Zhu, T., Zhang, Q., & Zhang, X. (2014). Pathways of
675 sulfate enhancement by natural and anthropogenic mineral aerosols in China. *Journal of*
676 *Geophysical Research-Atmospheres, 119*(24), 14165-14179. doi:10.1002/2014jd022301
677 Hussain, R., & Lun, K. (2019). The Geological Availability and Emissions of Sulfur and SO_2
678 from the Typical Coal of China. *Aerosol and Air Quality Research, 19*(3), 559-570.
679 doi:10.4209/aaqr.2018.08.0281
680 Intergovernmental Panel on Climate, C. (2014). *Climate Change 2013 – The Physical Science*
681 *Basis: Working Group I Contribution to the Fifth Assessment Report of the Intergovernmental*
682 *Panel on Climate Change*. Cambridge: Cambridge University Press.
683 Itahashi, S. (2018). Toward Synchronous Evaluation of Source Apportionments for Atmospheric
684 Concentration and Deposition of Sulfate Aerosol Over East Asia. *Journal of Geophysical*
685 *Research-Atmospheres, 123*(5), 2927-2953. doi:10.1002/2017jd028110
686 Itahashi, S., Yumimoto, K., Uno, I., Hayami, H., Fujita, S.-i., Pan, Y., & Wang, Y. (2018). A 15-
687 year record (2001-2015) of the ratio of nitrate to non-sea-salt sulfate in precipitation over East
688 Asia. *Atmospheric Chemistry and Physics, 18*(4), 2835-2852. doi:10.5194/acp-18-2835-2018
689 Jo, Y.-J., Lee, H.-J., Jo, H.-Y., Woo, J.-H., Kim, Y., Lee, T., . . . Kim, C.-H. (2020). Changes in
690 inorganic aerosol compositions over the Yellow Sea area from impact of Chinese emissions
691 mitigation. *Atmospheric Research, 240*. doi:10.1016/j.atmosres.2020.104948
692 Karplus, V. J., Zhang, S., & Almond, D. (2018). Quantifying coal power plant responses to
693 tighter SO_2 emissions standards in China. *Proceedings of the National Academy of Sciences of*
694 *the United States of America, 115*(27), 7004-7009. doi:10.1073/pnas.1800605115
695 Kasoar, M., Voulgarakis, A., Lamarque, J.-F., Shindell, D. T., Bellouin, N., Collins, W. J., . . .
696 Tsigaridis, K. (2016). Regional and global temperature response to anthropogenic SO_2 emissions

from China in three climate models. *Atmospheric Chemistry and Physics, 16*(15), 9785-9804. doi:10.5194/acp-16-9785-2016

Keene, W. C., Galloway, J. N., Likens, G. E., Deviney, F. A., Mikkelsen, K. N., Moody, J. L., & Maben, J. R. (2015). Atmospheric Wet Deposition in Remote Regions: Benchmarks for Environmental Change. *Journal of the Atmospheric Sciences, 72*(8), 2947-2978. doi:10.1175/jas-d-14-0378.1

Kipling, Z., Stier, P., Johnson, C. E., Mann, G. W., Bellouin, N., Bauer, S. E., . . . Zhang, K. (2016). What controls the vertical distribution of aerosol? Relationships between process sensitivity in HadGEM3-UKCA and inter-model variation from AeroCom Phase II. *Atmospheric Chemistry and Physics, 16*(4), 2221-2241. doi:10.5194/acp-16-2221-2016

Lamarque, J. F., Emmons, L. K., Hess, P. G., Kinnison, D. E., Tilmes, S., Vitt, F., . . . Tyndall, G. K. (2012). CAM-chem: description and evaluation of interactive atmospheric chemistry in the Community Earth System Model. *Geoscientific Model Development, 5*(2), 369-411. doi:10.5194/gmd-5-369-2012

Lee, H.-J., Jo, H.-Y., Song, C.-K., Jo, Y.-J., Park, S.-Y., & Kim, C.-H. (2020). Sensitivity of Simulated $PM_{2.5}$ Concentrations over Northeast Asia to Different Secondary Organic Aerosol Modules during the KORUS-AQ Campaign. *Atmosphere, 11*(9). doi:10.3390/atmos11091004

Li, B., Gasser, T., Ciais, P., Piao, S., Tao, S., Balkanski, Y., . . . Zhou, F. (2016). The contribution of China's emissions to global climate forcing. *Nature, 531*(7594), 357-+. doi:10.1038/nature17165

Li, B., Wang, X., Lei, R., Li, X., Li, W., & Fu, B. (2018). Numerical Simulation of Sulfate and Black Carbon Pollution in East Asia. [东亚硫酸盐及黑碳污染特征数值模拟]. *Environmental Science and Technology, 41*(5), 138-145. Retrieved from <Go to ISI>://CSCD:6257438

720 Li, G., Bei, N., Cao, J., Huang, R., Wu, J., Feng, T., . . . Molina, L. T. (2017). A possible
721 pathway for rapid growth of sulfate during haze days in China. *Atmospheric Chemistry and*
722 *Physics, 17*(5), 3301-3316. doi:10.5194/acp-17-3301-2017
723 Li, H., Cheng, J., Zhang, Q., Zheng, B., Zhang, Y., Zheng, G., & He, K. (2019). Rapid transition
724 in winter aerosol composition in Beijing from 2014 to 2017: response to clean air actions.
725 *Atmospheric Chemistry and Physics, 19*(17), 11485-11499. doi:10.5194/acp-19-11485-2019
726 Li, J., Zhang, Y.-L., Cao, F., Zhang, W., Fan, M., Lee, X., & Michalski, G. (2020). Stable Sulfur
727 Isotopes Revealed a Major Role of Transition-Metal Ion-Catalyzed SO_2 Oxidation in Haze
728 Episodes. *Environmental Science & Technology, 54*(5), 2626-2634. doi:10.1021/acs.est.9b07150
729 Li, X., & Liu, Y. (2013). Assessment of Two Aerosol Modules of CAM5. [Cam5 模式中两气溶
730 胶模块的评估]. *Journal of Applied Meteorolgical Science, 24*(1), 75-86. Retrieved from <Go to
731 ISI>://CSCD:4771081
732 Li, X., Zhao, B., Zhou, W., Shi, H., Yin, R., Cai, R., . . . Jiang, J. (2020). Responses of gaseous
733 sulfuric acid and particulate sulfate to reduced SO_2 concentration: A perspective from long-term
734 measurements in Beijing. *Science of the Total Environment, 721*.
735 doi:10.1016/j.scitotenv.2020.137700
736 Liu, B., Wu, J., Zhang, J., Wang, L., Yang, J., Liang, D., . . . Zhang, Q. (2017). Characterization
737 and source apportionment of $PM_{2.5}$ based on error estimation from EPA PMF 5.0 model at a
738 medium city in China. *Environmental Pollution, 222*, 10-22. doi:10.1016/j.envpol.2017.01.005
739 Liu, J., Fan, S., Horowitz, L. W., & Levy, H., II. (2011). Evaluation of factors controlling long-
740 range transport of black carbon to the Arctic. *Journal of Geophysical Research-Atmospheres,*
741 *116*. doi:10.1029/2010jd015145

742 Liu, L., Shawki, D., Voulgarakis, A., Kasoar, M., Samset, B. H., Myhre, G., . . . Takemura, T.
743 (2018). A PDRMIP Multimodel Study on the Impacts of Regional Aerosol Forcings on Global
744 and Regional Precipitation. *Journal of Climate, 31*(11), 4429-4447. doi:10.1175/jcli-d-17-0439.1
745 Liu, M., & Matsui, H. (2021). Aerosol radiative forcings induced by substantial changes in
746 anthropogenic emissions in China from 2008 to 2016. *Atmospheric Chemistry and Physics,*
747 *21*(8), 5965-5982. doi:10.5194/acp-21-5965-2021
748 Liu, M., Song, Y., Xu, T., Xu, Z., Wang, T., Yin, L., . . . Tang, J. (2020). Trends of Precipitation
749 Acidification and Determining Factors in China During 2006-2015. *Journal of Geophysical*
750 *Research-Atmospheres, 125*(6). doi:10.1029/2019jd031301
751 Liu, X., Easter, R. C., Ghan, S. J., Zaveri, R., Rasch, P., Shi, X., . . . Mitchell, D. (2012). Toward
752 a minimal representation of aerosols in climate models: description and evaluation in the
753 Community Atmosphere Model CAM5. *Geoscientific Model Development, 5*(3), 709-739.
754 doi:10.5194/gmd-5-709-2012
755 Liu, X., Penner, J. E., Das, B., Bergmann, D., Rodriguez, J. M., Strahan, S., . . . Feng, Y. (2007).
756 Uncertainties in global aerosol simulations: Assessment using three meteorological data sets.
757 *Journal of Geophysical Research-Atmospheres, 112*(D11). doi:10.1029/2006jd008216
758 Lu, X., Fung, J. C. H., & Wu, D. (2015). Modeling wet deposition of acid substances over the
759 PRD region in China. *Atmospheric Environment, 122*, 819-828.
760 doi:10.1016/j.atmosenv.2015.09.035
761 Luo, G., Yu, F., & Moch, J. M. (2020). Further improvement of wet process treatments in
762 GEOS-Chem v12.6.0: impact on global distributions of aerosols and aerosol precursors.
763 *Geoscientific Model Development, 13*(6), 2879-2903. doi:10.5194/gmd-13-2879-2020

764 Ma, X.-x., Liu, H.-n., Wang, X.-y., & Zhang, R.-j. (2016). THE RADIATIVE EFFECTS OF
765 ANTHROPOGENIC AEROSOLS OVER CHINA AND THEIR SENSITIVITY TO SOURCE
766 EMISSION. *Journal of Tropical Meteorology, 22*(1), 94-108. Retrieved from <Go to
767 ISI>://WOS:000371651900011

768 Ma, X., Shi, G., Guo, Y., & Wang, X. (2005). RADIATIVE FORCING BY GREENHOUSE
769 GASES AND SULFATE AEROSOL. [温室气体和硫酸盐气溶胶的辐射强迫作用]. *Acta*
770 *Meteorologica Sinica, 63*(1), 41-48. Retrieved from <Go to ISI>://CSCD:1868240

771 Matus, A. V., L'Ecuyer, T. S., & Henderson, D. S. (2019). New Estimates of Aerosol Direct
772 Radiative Effects and Forcing From A-Train Satellite Observations. *Geophysical Research*
773 *Letters, 46*(14), 8338-8346. doi:10.1029/2019gl083656

774 McClure, C. D., & Jaffe, D. A. (2018). US particulate matter air quality improves except in
775 wildfire-prone areas. *Proceedings of the National Academy of Sciences of the United States of*
776 *America, 115*(31), 7901-7906. doi:10.1073/pnas.1804353115

777 McDuffie, E. E., Smith, S. J., O'Rourke, P., Tibrewal, K., Venkataraman, C., Marais, E. A., . . .
778 Martin, R. V. (2020). A global anthropogenic emission inventory of atmospheric pollutants from
779 sector- and fuel-specific sources (1970-2017): an application of the Community Emissions Data
780 System (CEDS). *Earth System Science Data, 12*(4), 3413-3442. doi:10.5194/essd-12-3413-2020

781 Ming, Y., Ramaswamy, V., Ginoux, P. A., Horowitz, L. W., & Russell, L. M. (2005).
782 Geophysical Fluid Dynamics Laboratory general circulation model investigation of the indirect
783 radiative effects of anthropogenic sulfate aerosol. *Journal of Geophysical Research-*
784 *Atmospheres, 110*(D22). doi:10.1029/2005jd006161

785 Molod, A., Takacs, L., Suarez, M., & Bacmeister, J. (2015). Development of the GEOS-5
786 atmospheric general circulation model: evolution from MERRA to MERRA2. *Geoscientific*
787 *Model Development, 8*(5), 1339-1356. doi:10.5194/gmd-8-1339-2015
788 Ni, M., Zheng, J., Ma, Y., Wang, L., & Wang, M. (2016). Research Progress in Radiative
789 Forcing of Aerosol. [气溶胶的辐射强迫作用研究进展]. *Environmental Science and*
790 *Technology, 39*(10), 73-78,112. Retrieved from <Go to ISI>://CSCD:5856358
791 Paulot, F., Paynter, D., Ginoux, P., Naik, V., & Horowitz, L. W. (2018). Changes in the aerosol
792 direct radiative forcing from 2001 to 2015: observational constraints and regional mechanisms.
793 *Atmospheric Chemistry and Physics, 18*(17), 13265-13281. doi:10.5194/acp-18-13265-2018
794 Penner, J. E., Chuang, C. C., & Grant, K. (1998). Climate forcing by carbonaceous and sulfate
795 aerosols. *Climate Dynamics, 14*(12), 839-851. doi:10.1007/s003820050259
796 Qiao, X., Xiao, W., Jaffe, D., Kota, S. H., Ying, Q., & Tang, Y. (2015). Atmospheric wet
797 deposition of sulfur and nitrogen in Jiuzhaigou National Nature Reserve, Sichuan Province,
798 China. *Science of the Total Environment, 511*, 28-36. doi:10.1016/j.scitotenv.2014.12.028
799 Richardson, T. B., Forster, P. M., Smith, C. J., Maycock, A. C., Wood, T., Andrews, T., . . .
800 Watson-Parris, D. (2019). Efficacy of Climate Forcings in PDRMIP Models. *Journal of*
801 *Geophysical Research-Atmospheres, 124*(23), 12824-12844. doi:10.1029/2019jd030581
802 Rogora, M., Colombo, L., Marchetto, A., Mosello, R., & Steingruber, S. (2016). Temporal and
803 spatial patterns in the chemistry of wet deposition in Southern Alps. *Atmospheric Environment,*
804 *146*, 44-54. doi:10.1016/j.atmosenv.2016.06.025
805 Sanchez, K. J., Chen, C.-L., Russell, L. M., Betha, R., Liu, J., Price, D. J., . . . Behrenfeld, M. J.
806 (2018). Substantial Seasonal Contribution of Observed Biogenic Sulfate Particles to Cloud
807 Condensation Nuclei. *Scientific Reports, 8*. doi:10.1038/s41598-018-21590-9

Sedefian, L., Ku, M., Civerolo, K., Hao, W., & Zalewsky, E. (2016, Oct 03-07, 2018). *Regional Refined Grid Modeling of Acidic and Mercury Deposition over Northeastern US and the Contribution of New York Power Point Sources.* Paper presented at the 35th International Technical Meeting on Air Pollution Modelling and its Application (ITM), Chania, GREECE.

Sha, T., Ma, X., Jia, H., Tian, R., Chang, Y., Cao, F., & Zhang, Y. (2019). Aerosol chemical component: Simulations with WRF-Chem and comparison with observations in Nanjing. *Atmospheric Environment, 218*. doi:10.1016/j.atmosenv.2019.116982

Shao, J., Chen, Q., Wang, Y., Lu, X., He, P., Sun, Y., . . . Alexander, B. (2019). Heterogeneous sulfate aerosol formation mechanisms during wintertime Chinese haze events: air quality model assessment using observations of sulfate oxygen isotopes in Beijing. *Atmospheric Chemistry and Physics, 19*(9), 6107-6123. doi:10.5194/acp-19-6107-2019

Shawki, D., Voulgarakis, A., Chakraborty, A., Kasoar, M., & Srinivasan, J. (2018). The South Asian Monsoon Response to Remote Aerosols: Global and Regional Mechanisms. *Journal of Geophysical Research-Atmospheres, 123*(20), 11585-11601. doi:10.1029/2018jd028623

Sickles, J. E., II, & Shadwick, D. S. (2015). Air quality and atmospheric deposition in the eastern US: 20 years of change. *Atmospheric Chemistry and Physics, 15*(1), 173-197. doi:10.5194/acp-15-173-2015

Smith, C. J., Kramer, R. J., Myhre, G., Alterskjaer, K., Collins, W., Sima, A., . . . Forster, P. M. (2020). Effective radiative forcing and adjustments in CMIP6 models. *Atmospheric Chemistry and Physics, 20*(16), 9591-9618. doi:10.5194/acp-20-9591-2020

Sobhani, N., Kulkarni, S., & Carmichael, G. R. (2018). Source sector and region contributions to black carbon and $PM_{2.5}$ in the Arctic. *Atmospheric Chemistry and Physics, 18*(24), 18123-18148. doi:10.5194/acp-18-18123-2018

831 Steven, J. S., Yuyu, Z., & Page, K. (2015). *A Community Emissions Data System (CEDS)*
832 *Emissions For CMIP6 and Beyond*. Paper presented at the 2015 International Emission
833 Inventory Conference, San Diego, CA.
834 Stevens, B. (2015). Rethinking the Lower Bound on Aerosol Radiative Forcing. *Journal of*
835 *Climate, 28*(12), 4794-4819. doi:10.1175/jcli-d-14-00656.1
836 Thornhill, G. D., Collins, W. J., Kramer, R. J., Olivi, D., Skeie, R. B., O'Connor, F. M., . . .
837 Zhang, J. (2021). Effective radiative forcing from emissions of reactive gases and aerosols - a
838 multi-model comparison. *Atmospheric Chemistry and Physics, 21*(2), 853-874. doi:10.5194/acp-
839 21-853-2021
840 Vivanco, M. G., Bessagnet, B., Cuvelier, C., Theobald, M. R., Tsyro, S., Pirovano, G., . . . Ung,
841 A. (2017). Joint analysis of deposition fluxes and atmospheric concentrations of inorganic
842 nitrogen and sulphur compounds predicted by six chemistry transport models in the frame of the
843 EURODELTAIII project. *Atmospheric Environment, 151*, 152-175.
844 doi:10.1016/j.atmosenv.2016.11.042
845 Wang, W., Liu, M., Wang, T., Song, Y., Zhou, L., Cao, J., . . . Ge, M. (2021). Sulfate formation
846 is dominated by manganese-catalyzed oxidation of SO_2 on aerosol surfaces during haze events.
847 *Nature Communications, 12*(1). doi:10.1038/s41467-021-22091-6
848 Wei, Y., Chen, X., Chen, H., Li, J., Wang, Z., Yang, W., . . . Huang, H. (2019). IAP-AACM
849 v1.0: a global to regional evaluation of the atmospheric chemistry model in CAS-ESM.
850 *Atmospheric Chemistry and Physics, 19*(12), 8269-8296. doi:10.5194/acp-19-8269-2019
851 Wofsy, S. C., Afshar, S., Allen, H. M., Apel, E. C., Asher, E. C., Barletta, B., . . . Vieznor, N.
852 (2021). ATom: Merged Atmospheric Chemistry, Trace Gases, and Aerosols, Version 2. In:
853 ORNL Distributed Active Archive Center.

Wu, T., Zhang, F., Zhang, J., Jie, W., Zhang, Y., Wu, F., . . . Hu, A. (2020). Beijing Climate Center Earth System Model version 1 (BCC-ESM1): model description and evaluation of aerosol simulations. *Geoscientific Model Development, 13*(3), 977-1005. doi:10.5194/gmd-13-977-2020

Xie, X., Liu, X., Wang, H., & Wang, Z. (2016). Effects of Aerosols on Radiative Forcing and Climate Over East Asia With Different SO_2 Emissions. *Atmosphere, 7*(8). doi:10.3390/atmos7080099

Xue, J., Yuan, Z., Griffith, S. M., Yu, X., Lau, A. K. H., & Yu, J. Z. (2016). Sulfate Formation Enhanced by a Cocktail of High NO_x, SO_2, Particulate Matter, and Droplet pH during Haze-Fog Events in Megacities in China: An Observation-Based Modeling Investigation. *Environmental Science & Technology, 50*(14), 7325-7334. doi:10.1021/acs.est.6b00768

Yan, X., & Xu, Y. (2021). SO_2 mitigation in China's coal-fired power plants: A satellite-based assessment on compliance and enforcement. *Atmospheric Environment, 254*. doi:10.1016/j.atmosenv.2021.118396

Yang, Y., Wang, H., Smith, S. J., Easter, R., Ma, P.-L., Qian, Y., . . . Rasch, P. J. (2017). Global source attribution of sulfate concentration and direct and indirect radiative forcing. *Atmospheric Chemistry and Physics, 17*(14), 8903-8922. doi:10.5194/acp-17-8903-2017

Yang, Y., Wang, H., Smith, S. J., Easter, R. C., & Rasch, P. J. (2018). Sulfate Aerosol in the Arctic: Source Attribution and Radiative Forcing. *Journal of Geophysical Research-Atmospheres, 123*(3), 1899-1918. doi:10.1002/2017jd027298

Yue, F., Xie, Z., Zhang, P., Song, S., He, P., Liu, C., . . . Kang, H. (2019). The role of sulfate and its corresponding S(IV)+NO_2 formation pathway during the evolution of haze in Beijing. *Science of the Total Environment, 687*, 741-751. doi:10.1016/j.scitotenv.2019.06.096

876 Zhang, B., Zhou, T., Liu, Y., Yan, C., Li, X., Yu, J., . . . Zheng, M. (2019). Comparison of water-
877 soluble inorganic ions and trace metals in $PM_{2.5}$ between online and offline measurements in
878 Beijing during winter. *Atmospheric Pollution Research, 10*(6), 1755-1765.
879 doi:10.1016/j.apr.2019.07.007
880 Zhang, F., Wang, Y., Peng, J., Chen, L., Sun, Y., Duan, L., . . . Zhang, R. (2020). An unexpected
881 catalyst dominates formation and radiative forcing of regional haze. *Proceedings of the National*
882 *Academy of Sciences of the United States of America, 117*(8), 3960-3966.
883 doi:10.1073/pnas.1919343117
884 Zhang, H., & Huang, J. (2014). Interpretation of the IPCC Fifth Assessment Report on
885 Anthropogenic and Natural Radiative Forcing. *Advances in Climate Change Research, 10*(1), 40-
886 44. doi:10.3969/j.issn.1673-1719.2014.01.009
887 Zheng, B., Zhang, Q., Zhang, Y., He, K. B., Wang, K., Zheng, G. J., . . . Kimoto, T. (2015).
888 Heterogeneous chemistry: a mechanism missing in current models to explain secondary
889 inorganic aerosol formation during the January 2013 haze episode in North China. *Atmospheric*
890 *Chemistry and Physics, 15*(4), 2031-2049. doi:10.5194/acp-15-2031-2015
891 Zheng, H., Song, S., Sarwar, G., Gen, M., Wang, S., Ding, D., . . . McElroy, M. B. (2020).
892 Contribution of Particulate Nitrate Photolysis to Heterogeneous Sulfate Formation for Winter
893 Haze in China. *Environmental Science & Technology Letters, 7*(9), 632-638.
894 doi:10.1021/acs.estlett.0c00368
895 Zheng, K., Zhao, T., Zhang, L., Zeng, N., Zheng, X., & Yang, Q. (2019). Characteristics of Wet
896 Deposition of Sulfate and Nitrate in Three Typical Cities in China in 2001-2017. [2001-2017 年
897 中国 3 个典型城市硫酸盐和硝酸盐湿沉降特征]. *Ecology and Environmental Sciences,*
898 *28*(12), 2390-2397. Retrieved from <Go to ISI>://CSCD:6643937

899 Zhou, S., Wu, L., Guo, J., Chen, W., Wang, X., Zhao, J., . . . Kuang, J. (2020). Measurement
900 report: Vertical distribution of atmospheric particulate matter within the urban boundary layer in
901 southern China - size-segregated chemical composition and secondary formation through cloud
902 processing and heterogeneous reactions. *Atmospheric Chemistry and Physics, 20*(11), 6435-
903 6453. doi:10.5194/acp-20-6435-2020

904

Journal of Geophysical Research: Atmospheres

Supporting Information for

Improvement and Uncertainties of Global Simulation of Sulfate Concentration and Radiative Forcing in CESM2

Wendong Ge[1], Junfeng Liu[1], Songlin Xiang[1], Yuhan Zhou[1], Jingcheng Zhou[1], Xiurong Hu[2], Jianmin Ma[1], Xuejun Wang[1], Yi Wan[1], Jianying Hu[1], Zhaobin Zhang[1], Xilong Wang[1], Shu Tao[1]

[1]Laboratory for Earth Surface Processes, College of Urban and Environmental Sciences, Peking University, Beijing, 100871, China

[2] College of Economics and Management, Nanjing University of Aeronautics and Astronautics, Nanjing, 211106, China

Contents of this file

Introduction

Figure S1 is monthly averaged surface sulfate concentrations in 2015. Figure S2 is vertical profiles of sulfate concentrations over different regions. Figure S3 is the differences in annual averaged sulfate radiative forcing between different cases in 2015. Figures S4 and S5 are the differences in annual global-mean sulfate radiative forcing distribution between the sensitivity tests and the Improved case in 2015. Table S1 is the description of all model simulations.

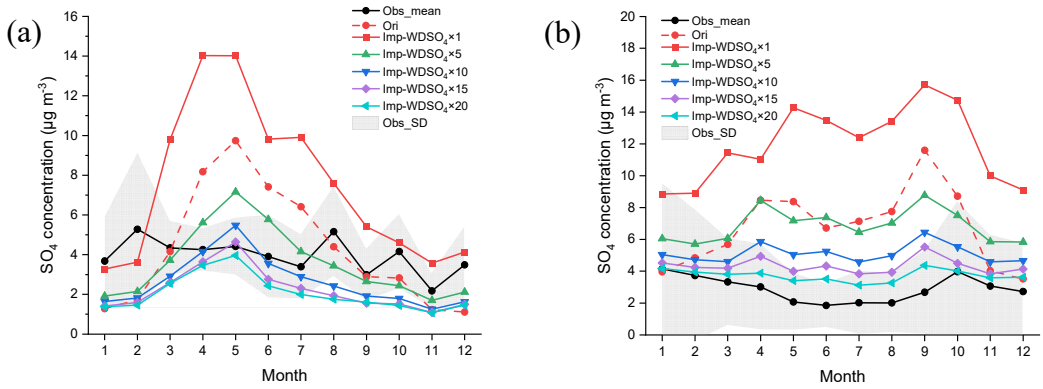

Figure S1. Monthly averaged surface sulfate concentrations (μg·m^{-3}) in (a) Japan and South Korea and (b) other Asia countries in 2015. The black solid lines and red dashed lines represent the observed and Original simulated concentrations, respectively. Other lines represent improved sulfate concentrations with different levels of sulfate wet deposition fluxes. The multiples of sulfate wet deposition from top to bottom are 1, 5, 10, 15 and 20 (i.e., the Improved case). The gray areas represent the standard deviation of the observed concentrations. The corresponding monitoring network is EANET.

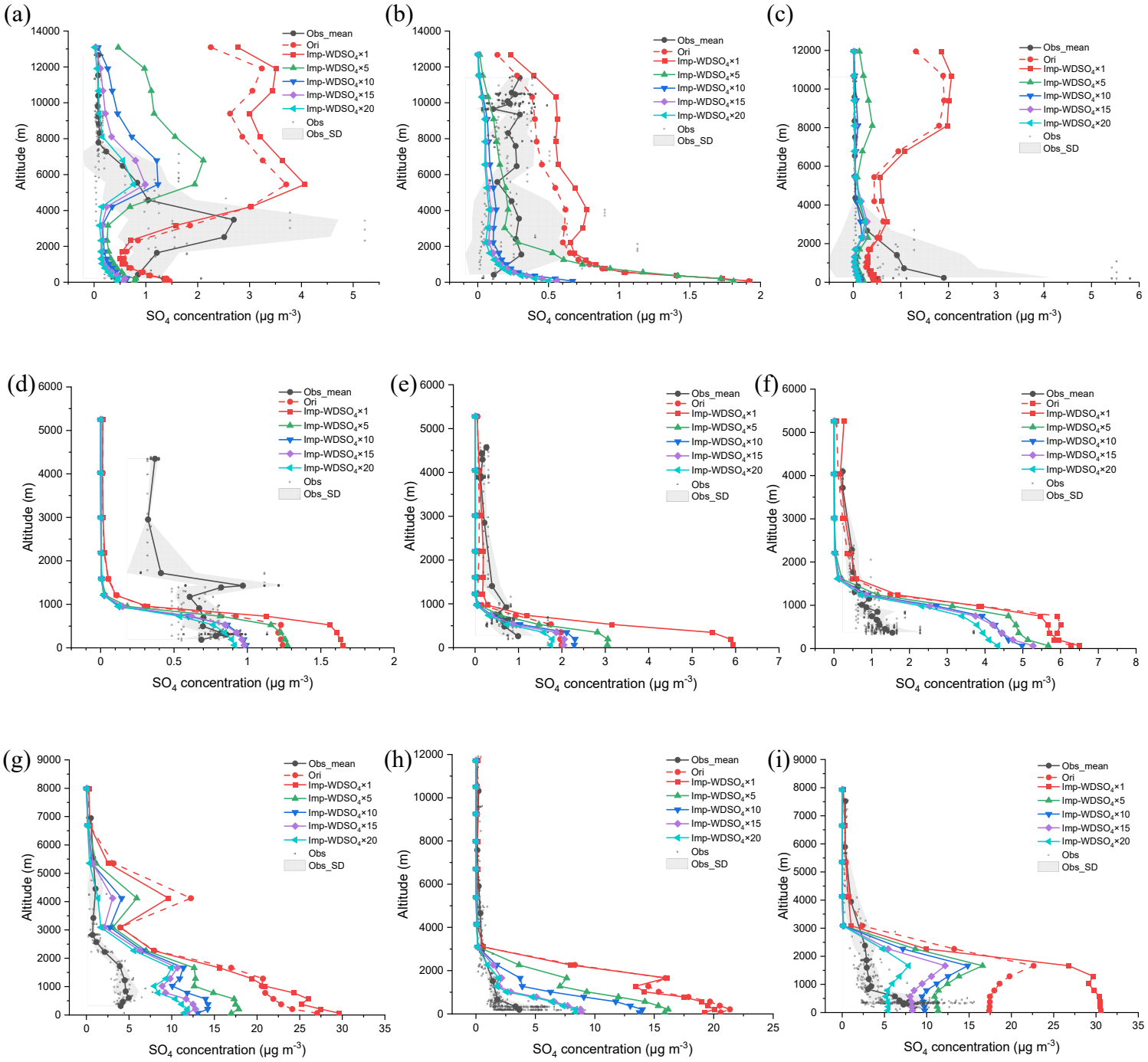

34

35 **Figure S2.** Vertical profiles of sulfate concentrations (μg·m^{-3}) over different regions. The black solid lines represent
36 the averaged observed concentrations at different altitudes. The red dashed lines represent the Original simulated
37 concentrations in the same day of 2015. Other lines represent improved sulfate concentrations with different levels
38 of sulfate wet deposition fluxes. The multiples of sulfate wet deposition from top to bottom are 1, 5, 10, 15 and 20
39 (i.e., the Improved case). The gray areas represent the standard deviation of observed concentrations. The black
40 dots represent every single observational data. The corresponding aircraft measurement campaigns are (a-c) ATom
41 on 29 July 2016, 1 August 2016 and 6 August 2016, (d-f) WINTER on 1 March 2015, 7 March 2015 and 12 March 2015
42 and (g-i) KORUS-AQ on 1 May 2016, 21 May 2016 and 4 June 2016.

43

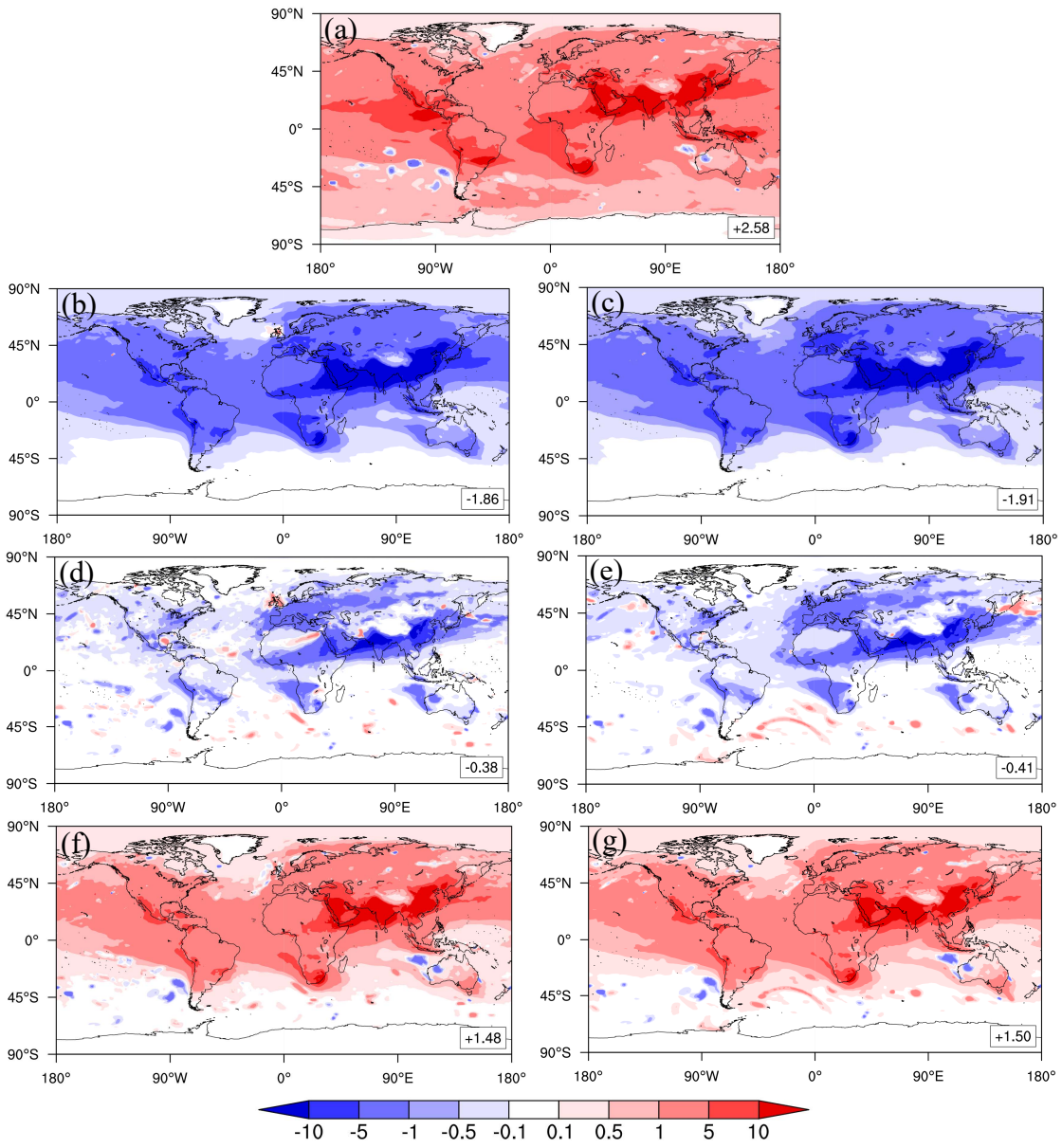

Figure S3. (a) The differences in annual averaged sulfate radiative forcing (unit: W· m^{-2}) between the Improved case and the Original case in 2015 after the incorporation of detailed in-cloud aqueous-phase chemical mechanisms and multiplication of the wet deposition flux of sulfate. (b) and (d) are the radiative forcing of Original simulated and Improved simulated sulfate from 1850 to 2015. (c) and (e) are the radiative forcing of Original simulated and Improved simulated sulfate from all anthropogenic emissions in 2015. (f) The differences in sulfate radiative forcing between (b) and (d). (g) The differences in sulfate radiative forcing between (c) and (e). The values in the corner are annual global-mean radiative forcing (unit: W· m^{-2}).

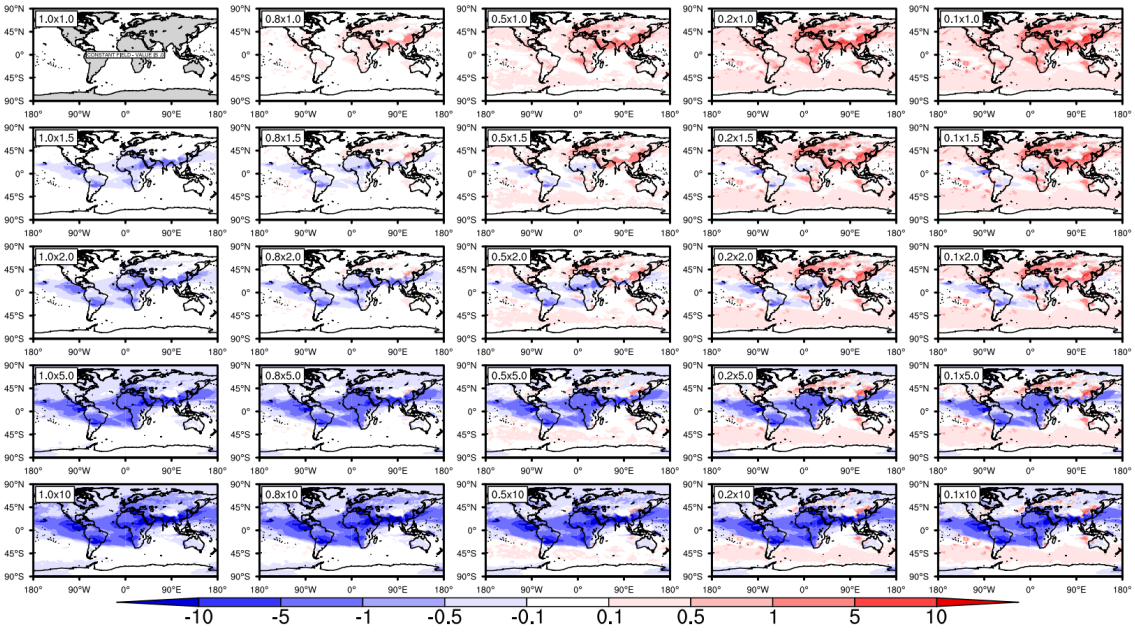

Figure S4. The differences in annual global-mean sulfate radiative forcing distribution (unit: $W \cdot m^{-2}$) between the sensitivity tests and the Improved case in 2015. The horizontal direction is the sensitivity test for decreasing the sulfate concentration at low altitudes (below 2.0 km). The decrease factors from left to right are 1.0, 0.8, 0.5, 0.2, and 0.1, indicating that the sulfate concentrations below 2.0 km are 100%, 80%, 50%, 20% and 10% of the Improved case, respectively. The vertical direction is the sensitivity test for increasing the sulfate concentration at high altitudes (above 2.0 km). The increase factors from top to bottom are 1.0, 1.5, 2.0, 5.0, and 10.

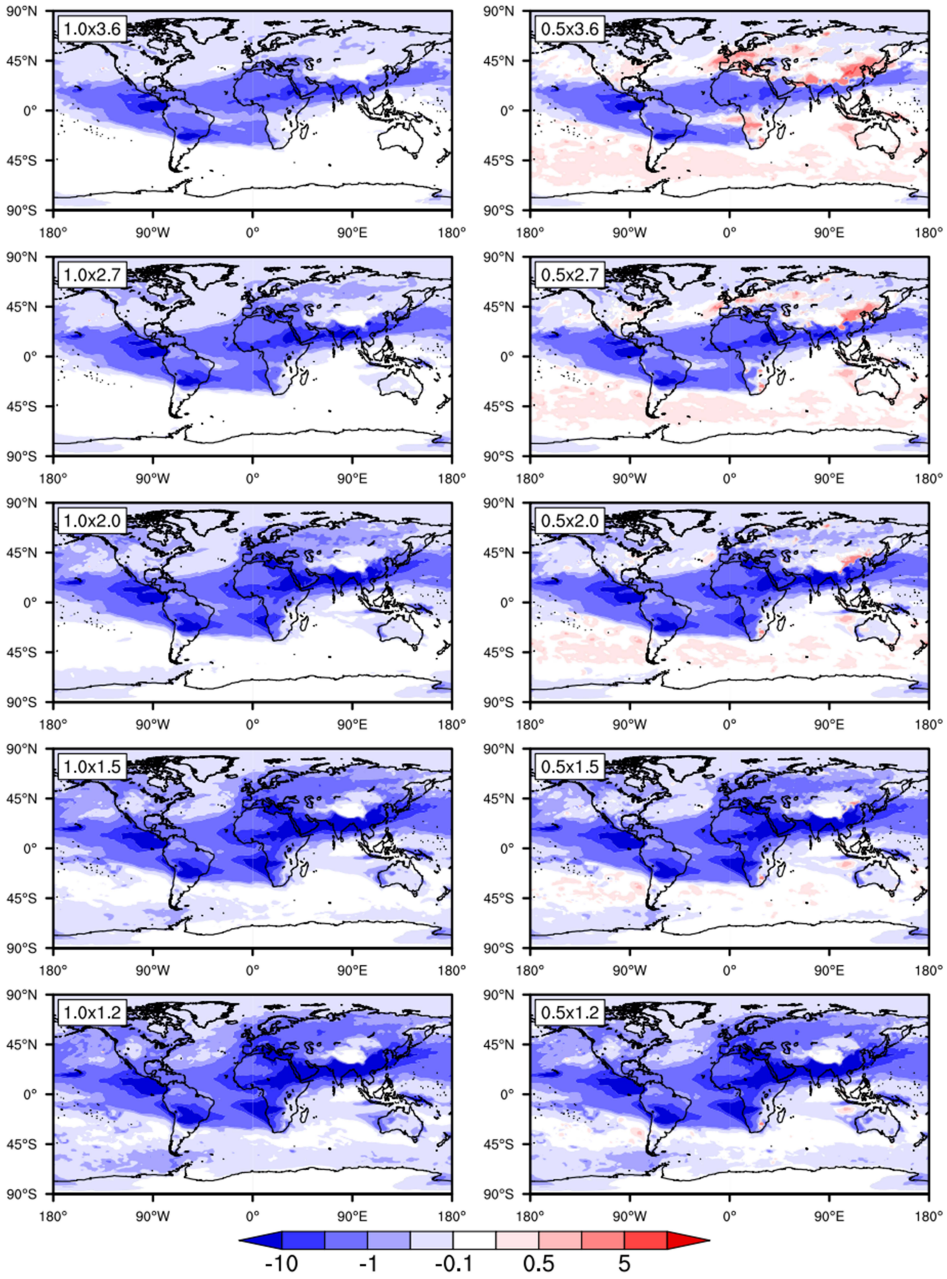

Figure S5. The differences in annual global-mean sulfate radiative forcing distribution (unit: $W \cdot m^{-2}$) between the sensitivity tests and the Improved case in 2015. The vertical direction is the sensitivity test for changing the altitude of the turning point (TP, the altitude above which the model tends to underestimate sulfate concentrations and below which the model tends to overestimate sulfate concentrations). The altitudes of the TP are set from bottom to top as 1.2, 1.5, 2.0, 2.7, and 3.6 km. The decreasing factors for sulfate concentration at low altitudes are 1.0 and 0.5, and the increasing factor for sulfate concentration at high altitudes is 10.

78 **Table S1.** Description of all model simulations.

No.	Case name	Location in the paper	Description
1	CESM-Ori	Sections 3.1, 3.2, 3.3	The present-day Original case without any modification to the model.
2~6	CESM-Imp-$WDSO_4$	Sections 3.1, 3.2, 3.3	The wet deposition of sulfate ×1, 5, 10, 15 and 20 (i.e., the present-day Improved case) with the incorporation of detailed in-cloud aqueous-phase chemical mechanisms, respectively.
7	CESM-Ori-1850		The preindustrial (1849-1850) Original case (only replaced the SO_2 emissions).
8	CESM-Imp-1850		The preindustrial Improved case.
9	CESM-Ori-anthro		The present-day Original case without any anthropogenic sources of sulfate.
10	CESM-Imp-anthro		The present-day Improved case without any anthropogenic sources of sulfate.
11	PORT-Ori	Sections 4.1, 4.2	The calculation of radiative forcing for case 1.
12	PORT-Imp	Sections 4.1, 4.2, 5	The calculation of radiative forcing for case 6.
13	PORT-Ori-1850	Section 4.2	The calculation of radiative forcing for case 7.
14	PORT-Imp-1850	Section 4.2	The calculation of radiative forcing for case 8.
15	PORT-Ori-anthro	Section 4.2	The calculation of radiative forcing for case 9.
16	PORT-Imp-anthro	Section 4.2	The calculation of radiative forcing for case 10.
17~20	PORT-high	Section 5	The calculation of radiative forcing when increasing the sulfate concentration (×1.5, 2.0, 5.0 and 10) at high altitudes.
21~24	PORT-low	Section 5	The calculation of radiative forcing when decreasing the sulfate concentration (×0.8, 0.5, 0.2 and 0.1) at low altitudes.
25~40	PORT-high×low	Section 5	The calculation of radiative forcing when increasing the sulfate concentration at high altitudes and decreasing the concentration at low altitudes simultaneously, including 1.5×0.8, 1.5×0.5, 1.5×0.2, 1.5×0.1, 2.0×0.8, 2.0×0.5, 2.0×0.2, 2.0×0.1, 5.0×0.8, 5.0×0.5, 5.0×0.2, 5.0×0.1, 10×0.8, 10×0.5, 10×0.2 and 10×0.1.
41~48	PORT-height	Section 5	The calculation of radiative forcing when changing the turning point.

79